RSC Advances

PAPER

View Article Online
View Journal | View Issue

Cite this: *RSC Adv.*, 2025, **15**, 46475

Liposomal formulation of *Fagonia arabica* L. enhances antithrombotic efficacy: phytochemical, pharmacological, and computational investigations

Sarah A. Badawy, *[a] Ahmed R. Hassan, [a] Medhat W. Shafaa,[b] Ahmed Mansour,[c] Marwa S. Abu Bakr[d] and Abd El-Salam I. Mohammed[e]

Fagonia arabica "Dhamasa" is traditionally used in Ayurvedic and Unani medicine across South Asia and the Middle East for its therapeutic properties, notably as a natural blood purifier. It is believed to aid in dissolving blood clots and reducing the risk of brain hemorrhage and cardiovascular events. Given previous reports of saponin content in *F. arabica*, this study aimed to evaluate its thrombolytic and anticoagulant potential. After confirming its saponin richness through NMR (1D, 2D) and LC-MS, we developed liposomal nanoparticles to enhance bioavailability and target clot dissolution more effectively. Liposomes were characterized using TEM, particle size, PDI, and zeta potential. *In vitro* thrombolytic and anticoagulant activities were assessed, followed by *in vivo* testing in adult Wistar rats. The dose-dependent effects of the saponin-rich *n*-butanol fraction of *F. arabica* on Antithrombin-III levels were evaluated using an *in vitro* quantitative immunoturbidimetric assay. Coagulation parameters were evaluated using aPTT and PT assays. A molecular docking study was systematically performed on nine targets using the five structurally elucidated steroidal and terpenoid glycosides to predict and evaluate their binding affinities. These computational findings were designed to complement ongoing *in vitro* and *in vivo* investigations. The butanol extract showed significant *in vitro* thrombolytic and anticoagulant effects at 40 mg mL^{-1}. The results demonstrate that the saponin-rich fraction modulates Antithrombin-III in a concentration-dependent manner. Liposomal nanoparticles achieved similar efficacy *in vivo* at just 3 mg kg^{-1}, compared to 100 mg kg^{-1} for the non-nano extract. The liposomal group showed PT of 35 ± 4 s and aPTT >180 s, outperforming the non-nano extract (PT 30 ± 7 s, aPTT >180 s) and controls (PT 12 ± 2 s, aPTT 37 ± 3 s). The docking study provides mechanistic insight into their potential multi-target antithrombotic activities. Besides the butanol extract, liposomal *F. arabica* enhances antithrombotic efficacy at lower doses, supporting its potential as a natural therapeutic candidate for thrombotic disorders.

Received 25th August 2025
Accepted 15th November 2025

DOI: 10.1039/d5ra06347g

rsc.li/rsc-advances

1 Introduction

The tropical shrub *Fagonia arabica*, also called "Dhamasa," belongs to the Zygophyllaceae family and is found throughout the Indian subcontinent, Mediterranean Africa, Afghanistan, and Pakistan. Many herbal formulations, including *F. arabica*, have been used in traditional Indian medicine, especially Ayurveda, for their neuroprotective qualities as well as to treat inflammatory, haematological, hepatic, and endocrinological conditions.[1–3] Typically reaching 1–3 feet in height and thriving on calcareous soils, this perennial green shrub is recognized for its broad spectrum of therapeutic applications. Different parts of the plant have traditionally been employed in the management of various ailments, including fever, smallpox, skin disorders, and as a blood purifier. Acting as a deobstruent, it is also valued for its cooling properties, particularly in oral inflammatory conditions such as stomatitis. *F. arabica* is rich in triterpenoid saponins and antioxidants, conferring significant medicinal potential. Traditionally, its branches have been applied in the treatment of snake bites and formulated as a paste to alleviate swellings and tumors, especially in the cervical region.[2]

A hydrophobic polycyclic aglycone core (sapogenin) is joined to one or more hydrophilic sugar moieties to form saponins, amphipathic glycosides that are distinguished by their distinctive foaming qualities. Notable antithrombotic potential is one of the many pharmacological effects facilitated by their distinct structural characteristics. Saponins are known for their

[a]*Medicinal and Aromatic Plants Department, Desert Research Center, El-Matariya 11753, Cairo, Egypt. E-mail: sarahahmed.2252@azhar.edu.eg; Tel: +201067276452*
[b]*Physics Department, Medical Biophysics Division, Faculty of Sciences, Helwan University, Helwan 11792, Cairo, Egypt*
[c]*Department of Pharmacology and Toxicology, Faculty of Pharmacy (for Boys), Al-Azhar University, Nasr City 13129, Cairo, Egypt*
[d]*Department of Pharmacognosy, Faculty of Pharmacy (for Girls), Al-Azhar University, Nasr City 11651, Cairo, Egypt*
[e]*Department of Pharmacognosy, Faculty of Pharmacy (for Boys), Al-Azhar University, Nasr City 13129, Cairo, Egypt*

ability to lyse erythrocytes, a property attributed to their interaction with membrane sterols, leading to increased permeability and irreversible damage to the lipid bilayer. This haemolytic activity serves as a useful bioassay for detecting saponins in plant extracts and pharmaceutical preparations. Studies confirmed that erythrocytes lysed by saponins do not reseal, supporting the notion of permanent membrane disruption.[4] The haemolytic effects of 47 plant-derived saponins were evaluated, and observed that although many exhibited haemolysis, adjuvant activity did not consistently correlate with haemolytic potential.[5] The haemolytic effect was found to be structure-dependent, influenced by the aglycone core and sugar moieties; particularly, the presence of acyl groups and oxide rings increased haemolytic potential, with exceptions such as lablaboside D. Strong haemolytic activity was reported for saponins from *Aesculus hippocastanum*, *Zizyphus jujuba*, and *Maesa lanceolata*, the latter showing 50% erythrocyte lysis at 1.6 mg mL^{-1}. Structural analysis revealed that substitution at C-22 is critical for the haemolytic potency of maesasaponins. Additionally, an oleanolic acid-based saponin mixture from *Pometia ridleyi* exhibited 70% haemolysis at 25 mg mL^{-1}, with HD_{50} at approximately 23 mg mL^{-1}. Further demonstrated that saikosaponins from *Bupleurum falcatum* not only exhibited strong haemolytic activity but also inhibited cell adhesion, suggesting a shared mechanism of membrane disruption underlying both effects.[6] There is growing evidence that several saponins have anticoagulant, antiplatelet, and anti-aggregatory properties that can alter the haemostatic system.[7] Certain saponins have an impact on prothrombin and other clotting factors, which are important components of the coagulation cascade. For example, Sapinmusaponins F–J have strong antiplatelet action at doses ranging from 1 to 100 μM in human *in vitro* experiments employing cleansed platelets.[8] Similarly, with reported IC_{50} values of roughly 3.4–13.5 μM and 30.5 μM, respectively, Sapinmusaponins *Q* and *R* (1–50 μM) demonstrated strong anti-aggregatory actions, outperforming aspirin in efficacy.[9] These results highlight the potential of particular saponins as natural remedies for thromboembolic disease prevention and treatment.

Developing a blood clot (thrombus) inside a blood vessel is known as thrombosis. This condition impairs normal blood flow and may result in tissue hypoxia or infarction in regions supplied by the obstructed channel. Depending on its location, a thrombus that separates and moves through the bloodstream can become an embolus, which may block vessels at distant sites and cause serious complications. Several risk factors, such as atrial fibrillation, prosthetic heart valves, myocardial infarction, prolonged immobility, and hereditary or acquired coagulation abnormalities, contribute to the formation of thrombi, although many eventually transform into fibrous tissue, and the vessel may recanalize. Because it dramatically reduces the chance of potentially fatal illnesses like stroke, myocardial infarction, and pulmonary embolism, thrombosis prevention is essential.[10,11]

To overcome the main drawbacks of traditional treatments, including their short plasma half-life, systemic toxicity, and elevated risk of bleeding, liposomes have shown great promise as vehicles for the targeted delivery of antithrombotic and thrombolytic drugs.[10] These biocompatible phospholipid vesicles can encapsulate protein-based medications, including streptokinase and tissue plasminogen activator (tPA), thereby improving their pharmacokinetics and bioavailability while shielding them from immunological reactions and enzymatic breakdown.[12] Studies have demonstrated that liposomal formulations can greatly increase therapeutic efficacy; for example, at a fifth of the dose, liposome-encapsulated tPA produced thrombolysis that was comparable to that of free tPA.[13] Additionally, liposomes can selectively accumulate at thrombus sites through mechanisms like receptor-mediated targeting or the enhanced permeability and retention (EPR) effect. By minimising off-target effects and enabling localised medication action, this tailored delivery helps to minimise systemic fibrinolysis and the related bleeding problems. Additionally, liposomal systems represent a highly versatile platform for enhancing the safety and efficacy of thrombolytic and anticoagulant therapies, owing to their flexible formulation, which enables the co-delivery of multiple drugs and sustained release profiles.[14]

Addressing the pathological challenge of thrombus formation and promoting the dissolution of pre-existing clots implicated in life-threatening thromboembolic disorders, we focused on key molecular targets spanning the coagulation cascade, platelet activation pathways, and fibrinolytic system. Nine therapeutic targets were selected based on their critical roles in hemostasis: anticoagulant targets included Thrombin (Factor IIa), which catalyzes the conversion of fibrinogen to fibrin; Antithrombin III, a serine protease inhibitor that neutralizes thrombin and Factor Xa, with activity enhanced by heparin;[15] Factor Xa, a pivotal enzyme responsible for thrombin generation;[16] and Vitamin K epoxide reductase (VKOR), the pharmacological target of warfarin that regulates the γ-carboxylation and activation of clotting factors II, VII, IX, and X.[17]

Antiplatelet targets encompassed Cyclooxygenase-1 (COX-1), which synthesizes thromboxane A_2 (TXA_2) to mediate platelet aggregation;[18] the $P2Y_{12}$ ADP receptor, a key receptor on platelets that amplifies ADP-mediated platelet activation;[19] and Phosphodiesterase (PDE), which modulates intracellular cAMP levels and thereby influences platelet inhibition.[20]

For thrombolytic modulation within the fibrinolytic pathway, Plasminogen, the inactive zymogen that is proteolytically converted into plasmin,[21] and Tissue Plasminogen Activator (tPA), which catalyzes this conversion,[13,22] were selected.

A molecular docking study was systematically performed on these nine targets using the five structurally elucidated steroidal and terpenoid glycosides to predict and evaluate their binding affinities. These computational findings were designed to complement ongoing *in vitro* and *in vivo* investigations, providing mechanistic insight into their potential multi-target antithrombotic activities.

This study exploits the intrinsic penetration and permeation capabilities of liposomes to prevent and dissolve thrombi by encapsulating a traditionally used medicinal plant with a long history of therapeutic application. In this work, liposomes are prepared under mild conditions, avoiding high temperatures to

preserve the integrity of the bioactive compounds. This study aims to elucidate the antithrombotic potential of the plant by assessing its thrombolytic and anticoagulant activities, characterizing key bioactive constituents, and validating their therapeutic relevance through *in silico* protein-target simulations.

2 Experimental

2.1. General experimental procedures

Analytical-grade solvents, including dichloromethane, *n*-hexane, ethyl acetate, *n*-butanol, methanol, and ethanol, were sourced from Sigma-Aldrich and Fisher Scientific (USA). Thin-layer chromatography (TLC) was conducted on Merck-precoated Silica gel 60 GF_{254} plates. Visualization of chromatographic spots was achieved by spraying the plates with 5% sulfuric acid in methanol, followed by heating at 100 °C. Preparative TLC (PTLC) was also performed using the same silica gel plates. For column chromatography (CC), various stationary phases were employed, including silica gel G_{60} (60–120 mesh, Merck, USA), reversed-phase C_{18} silica gel (15–25 μm particle size, 100 Å pore size, Fluka, Switzerland), and Sephadex LH-20 (Merck, USA). Nuclear magnetic resonance (NMR) spectra, including both 1D and 2D experiments, were obtained on a Bruker 400 MHz spectrometer (400 MHz for ^{1}H and 101 MHz for ^{13}C) using pyridine-d_5 and CD_3OD as solvents. Mass spectrometric analyses were conducted *via* direct infusion using a Waters XEVO TQ-S mass spectrometer (Waters, USA) with electrospray ionization in positive and negative modes.

2.2. Plant material

During the flowering stage in March 2023, aerial portions of *Fagonia arabica* L. (Family: Zygophyllaceae) were collected in the Eastern Desert of Egypt (GPS coordinates: 25°55′–26°00′ N, 32°50′–33°00′ E).[23] Prof. Dr Abd El-Halim Abd El-Mogali Mohamed of the Flora and Phytotaxonomy Research Department of the Agricultural Museum in Dokki, Giza, Egypt, confirmed the plant specimen, and a voucher specimen of the plant (CAIM-29-3-2023/1) was kept in the herbarium of the Agricultural Museum in Egypt.

2.3. Extraction and fractionation by liquid–liquid partition chromatography

A total of 1.5 kg of air-dried and powdered aerial parts of *Fagonia arabica* L. underwent exhaustive extraction *via* maceration using 80% methanol (4 × 3 L). The combined hydro-methanolic extracts were filtered and concentrated under reduced pressure at 40 °C using a rotary evaporator, yielding 146 g of dried extract. This crude extract was suspended in 500 mL of distilled water and successively partitioned with *n*-hexane, dichloromethane (DCM), ethyl acetate (EtOAc), and n-butanol (each 3 × 1 L). The DCM, EtOAc, and butanol fractions were filtered and dried under reduced pressure.[24]

2.4. Reagents and chemicals for *in vitro* biological evaluation

All the chemicals and reagents used in the *in vitro* thrombolytic and anticoagulant tests were of analytical grade and were obtained from Sigma-Aldrich USA. Methanol, DCM, *n*-butanol, and ethyl acetate were the reagents used. Heparin calcium (5000 I.U./vial) from Amoun Pharmaceutical Company, Egypt, was used as a positive control, and normal saline was used as a negative control.

2.5. *In vitro* thrombolytic test

To evaluate the thrombolytic activity of *Fagonia arabica* extracts, 200 mg of each extract was suspended in 10 mL of normal saline, vigorously shaken, and left overnight. The mixture was decanted to collect the aqueous supernatant. A 100 μL aliquot of each extract was added to pre-formed blood clots in microcentrifuge tubes. The assay followed a modified version of a reported method, with normal saline used as the negative control instead of distilled water to minimize the risk of hemolysis.[25] All procedures involving human participants, including blood sample collection, were conducted in accordance with the ethical standards of the Declaration of Helsinki. Ethical approval was obtained from the Research Ethics Committee of the Faculty of Pharmacy for Girls, Al-Azhar University, Egypt (Ethics Approval No. 548). Informed consents were obtained from all participants before sample collection.

Fresh whole blood (5 mL) was obtained from three healthy volunteers who had not taken anticoagulants or contraceptives for at least seven days. Aliquots of 0.5 mL were distributed into seven pre-weighed (W1) sterile microcentrifuge tubes and incubated at 37 °C for 1 hour to allow clot formation. After clotting, serum was carefully removed, and the weight of the clot (ΔW) was determined as the difference between the weight of the tube containing the clot (W2) and the empty tube (W1). Each clot was then treated with 100 μL of either the plant extract, heparin (positive control), or normal saline (negative control) and incubated again at 37 °C for 90 minutes. Post-incubation, the tubes were reweighed to assess clot dissolution. The percentage of clot lysis was calculated using the formula:

$$\%\ \text{Clot lysis} = [(\text{weight of clot before lysis} - \text{weight after lysis})/\text{weight before lysis}] \times 100.$$

Each test was performed in triplicate using samples from all three volunteers.

2.6. *In vitro* anticoagulant test

The objective of this experiment was to assess the anticoagulant potential of *Fagonia arabica* total extract and its various fractions by evaluating their ability to inhibit blood clot formation, in comparison to heparin. Six concentrations (15, 30, 40, 50, 100, and 200 mg) of each sample were suspended in 1 mL of normal saline, vigorously shaken, and left overnight. The resulting suspensions were decanted, and 100 μL of each supernatant was transferred into microcentrifuge tubes before the addition of blood. Blood samples (4.5 mL) were collected from a healthy volunteer and divided into nine sterile microcentrifuge tubes, each receiving 0.5 mL of blood. Experimental

tubes contained the test samples, while controls were set as follows: one tube with 500 μL of blood alone (untreated control), another with 100 μL saline added to 500 μL blood (negative control), and a positive control consisting of 25 μL heparin mixed with 75 μL saline added to 500 μL blood. All tubes were standardized to a final volume of 600 μL to ensure consistency across samples. Clot formation was monitored for 24 hours, and clot weight was determined by carefully transferring the formed clots onto aluminum foil and weighing them. The experiment was conducted in triplicate using blood samples from three healthy donors to ensure reproducibility and statistical validity. All procedures were performed in accordance with the ethical standards of the Declaration of Helsinki. Ethical approval was obtained from the Research Ethics Committee of the Faculty of Pharmacy for Girls, Al-Azhar University, Egypt (Ethics Approval No. 548). Informed consents were obtained from all participants before sample collection.

2.7. Quantitative *in vitro* determination of antithrombin-III by immunoturbidimetric assay

Antithrombin-III (AT-III) was quantified using the QCA Antithrombin-III Quantitative Turbidimetry Kit (QCA Diagnostics- Spain) according to the manufacturer's protocol.[26] The supplied calibrator was used to prepare a series of working standards by mixing the calibrator with physiological saline as directed in the kit instructions. Each standard was freshly prepared and thoroughly mixed before analysis.

The saponin-rich butanol fraction was prepared by dissolving 6 mg of saponin in 0.5 mL of 0.9% saline, yielding a stock concentration of 12 mg mL^{-1}. From this stock, 5 μL was diluted with 4 mL of saline to obtain a working solution of approximately 0.015 mg mL^{-1} (15 μg mL^{-1}), equivalent to 0.015 μg of saponin per microliter. A series of reaction mixtures was prepared to evaluate the effect of the saponin-rich fraction on plasma antithrombin-III activity. The standard control (without plant extract) contained only 5 μL of citrated human plasma. Test samples were prepared by mixing 5 μL of plasma with increasing volumes of the saponin-rich fraction, specifically 5, 10, 20, 100, 200, and 500 μL, respectively. Each mixture was adjusted to the same final volume with saline before assay to ensure comparability among samples. The turbidimetric assay was performed by dispensing appropriate volumes of standards, controls, and test samples into cuvettes, then adding the QCA reagents in the order specified by the manufacturer. The reaction mixtures were done at 37 °C, and absorbance was measured at 340 nm using a calibrated spectrophotometer. The change in absorbance (ΔAbs) was recorded after 5 minutes of incubation.

Calibration standards' absorbance values were plotted against their corresponding concentrations to generate a standard curve, producing a linear regression equation:

Abs = 8.285 × C − 0.381, where C represents the AT-III concentration in mg dL^{-1}. Antithrombin-III concentrations were calculated using the inverse equation:

$$C\left(\frac{\text{mg}}{\text{d}L}\right) = \frac{\text{Abs} + 0.381}{8.285}.$$

All measurements were performed in triplicate to ensure accuracy and reproducibility.

2.8. Statistical analysis

The percentage of clot lysis induced by heparin and the herbal extracts was determined using the weight difference method, and the results are presented as mean ± SD for $n = 3$.

2.9. Encapsulation of *F. arabica* saponins from the butanol fraction in liposomal nanoparticles

2.9.1 Materials. Absolute ethanol (99.9%) was bought from DaeJung Chemicals (Seohaean-ro, Gyeonggi-do, Korea). L-α-phosphatidyl choline (Soy Lecithin) was purchased from Carl Roth (Karlsruhe, Germany) with a molecular weight of 760 in powder form and a purity of ≥97% (Fig. 1). Phosphate buffer saline was sourced from CDH, New Delhi, India. All solutions were prepared using distilled ultra-pure water, and all solvents and reagents were of HPLC grade.

2.9.2 Preparation of liposomal nanoparticles. Soy lecithin and *Fagonia arabica* at a weight ratio (w/w) of 7 : 2 were used to prepare neutral multilamellar vesicles (MLVs) using the thin-film hydration method of Bangham.[27] A total of 100 mg of soy lecithin and 28.6 mg of *Fagonia arabica* were transferred to a 100 mL round-bottom flask. Subsequently, 25 mL of ethanol (EtOH) was added, and the flask was gently shaken until all components were completely dissolved. The organic solvent was then gradually removed using a rotary evaporator under vacuum in a warm water bath (45 °C), resulting in the formation of a uniform thin lipid film on the inner wall of the flask. The lipid film was hydrated with phosphate-buffered saline (PBS, pH 7.4 at 37 °C) in a water bath at 45 °C for 15 min to form MLVs. The flask was then mechanically shaken at 45 °C for 1 h. Afterwards, it was flushed with a stream of nitrogen and immediately sealed. Empty liposomes, serving as controls, were prepared using the same procedure described above but with only soy lecithin in the same mass aliquots used for the formulation.[27]

2.9.3 Transmission electron microscopy (TEM). For morphological analysis, a drop of the liposomal suspension was placed on carbon-coated copper grids and allowed to air dry. TEM imaging was performed using a JEOL JEM-1010 transmission electron microscope operating at 80 kV at the Regional Centre for Mycology and Biotechnology (RCMB), Al-Azhar University.[28]

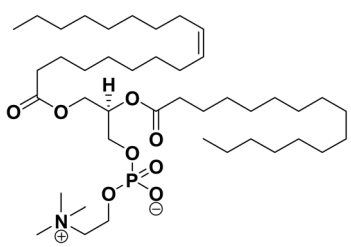

Fig. 1 Schematic chemical structure of L-α-phosphatidyl choline (Soy Lecithin).

2.9.4 Particle size and zeta potential analysis. Before measurement, samples were sonicated for 2 minutes. Particle size distribution and polydispersity index (PDI) were determined after one week of liposomal preparation using dynamic light scattering (DLS) on a Zetasizer Nano ZN (Malvern Panalytical, UK) at a fixed scattering angle of 173° and a temperature of 25 °C. Zeta potential was measured using the same instrument. All measurements were performed in triplicate.

2.10. Assay of the anticoagulant activity

2.10.1 Animals. Adult Wistar rats of both sexes, weighing between 180–220 g, were maintained under standard laboratory conditions, including a controlled temperature of 24 ± 2 °C and a 12-hours light/dark cycle beginning at 7:00 a.m. Animals had free access to standardized commercial feed and water. The experimental protocol was reviewed and approved by the Research Ethics Committee of the Faculty of Pharmacy (Girls), Al-Azhar University, Egypt (Ethics Approval No. 548). All experiments were performed in accordance with ARRIVE guidelines. Animals were obtained, bred, and housed in the Animal Facility of the Faculty of Pharmacy, Al-Azhar University. Rats were randomly assigned to three groups ($n = 5$ per group), with each animal serving as its own control before treatment. The groups included: a liposomal formulation group (3 mg kg^{-1}), a butanol extract group at 100 mg kg^{-1}, and a second butanol extract group at 200 mg kg^{-1}. Treatments were administered *via* injection, and pre- and post-treatment assessments were conducted for each group.

2.10.2 *Ex vivo* coagulation assay. The anticoagulant potential of *Fagonia arabica*'s most active butanol fraction and its liposomal nanoformulation was evaluated by measuring activated partial thromboplastin time (aPTT) and prothrombin time (PT) in rat plasma.[29] The formulations were administered *via* a single intraperitoneal (IP) injection at doses of 3 mg kg^{-1} (liposomal form), 100 mg kg^{-1} and 200 mg kg^{-1} (butanol extract). Blood samples (4 mL) were collected from anesthetized rats both before and 3 hours after administration, using syringes containing 3.8% sodium citrate as an anticoagulant. Plasma samples (platelet-poor plasma, PPP) were prepared by centrifugation at 2500×*g* for 15 minutes and used for coagulation analysis.[30]

2.11. LC-MS/MS analysis of *Fagonia arabica* butanol extract (the most biologically active fraction)

A total of 50 mg of the dried *n*-butanol extract was dissolved in 1 mL of a reconstitution solvent (H_2O : MeOH : MeCN, 50 : 25 : 25 v/v), followed by vortexing, ultrasonication, and centrifugation to ensure complete solubility. The solution was diluted to a final concentration of 2.5 μg μL^{-1}, and 10 μL was injected in both positive and negative ionization modes. Electrospray ionization mass spectrometry (ESI-MS) was performed in both positive and negative ion acquisition modes using a XEVO TQD triple quadrupole mass spectrometer (Waters Corporation, Milford, MA, USA). Chromatographic separation was achieved on an ACQUITY UPLC BEH C18 column (1.7 μm, 2.1 × 50 mm) operated at a flow rate of 0.2 mL min^{-1}. The mobile phase consisted of solvent A (water with 0.1% formic acid) and solvent B (acetonitrile with 0.1% formic acid). Gradient elution was applied as follows: the run commenced with 90 : 10% (A: B) from 0 to 4 min, followed by a shift to 70 : 30% from 5 to 14 min. The composition was then adjusted to 30 : 70% between 15 and 21 min, followed by 10 : 90% from 22 to 25 min. From 26 to 31 min, the gradient reached 100% solvent B, and finally returned to the initial 90 : 10% (A: B) at 32 min for re-equilibration.[31]

2.12. Isolation and purification of the major active constituents of the most biologically active fraction

By precipitation from the *n*-butanol fraction, compound **1** (20 mg) was yielded *via* crystallization, followed by further purification using Sephadex LH-20 gel filtration chromatography, eluted with 100% methanol. The *n*-butanol fraction (30 g) was subjected to polyamide column chromatography, eluted with a methanol–water gradient (100 : 0 to 30 : 70), resulting in five pooled subfractions (Bu-I to Bu-V) based on TLC profiles. Subfraction Bu-II, eluted with H_2O: MeOH (95 : 5), contained compounds **2** and **3**, while Bu-III, eluted with H_2O: MeOH (90 : 10), contained compounds **4** and **5**. Further purification of butanol subfractions was achieved using sequential chromatographic techniques, including silica gel column chromatography (EtOAc: MeOH: H_2O, 30 : 5:4), reversed-phase C18 column chromatography (H_2O: MeOH, 95 : 5), and final purification by Sephadex LH-20 gel filtration with 100% methanol, affording compounds **2** and **3** (16 mg) and compounds **4** and **5** (10 mg).[24]

2.13. *In silico* study

2.13.1 Molecular docking. To evaluate the binding affinities and interaction profiles of five selected terpenoid and steroidal glycosides with nine target proteins, molecular docking was performed at their respective allosteric binding sites. The protein targets were categorized into three functional groups: four anticoagulant targets: Thrombin (Factor IIa, PDB: 1PPB), Factor Xa (PDB: 2P16), Antithrombin III (PDB: 1AZX), and Vitamin K epoxide reductase (VKORC1, PDB: 6WV4); three antiplatelet targets: Cyclooxygenase-1 (COX-1/PTGS1, PDB: 1PTH), the P2Y12 receptor (PDB: 4NTJ), and Phosphodiesterase III (PDE3A, PDB: 1SO2); and two thrombolytic (fibrinolytic) targets: Plasminogen (PDB: 4DUU) and Tissue Plasminogen Activator (tPA, PDB: 1A5H). Docking simulations were conducted using AutoDock Vina, while the 3D structures of the ligands were retrieved from PubChem and Chem3D Ultra 8.0. Before docking, energy minimization and protonation optimization were performed using Chimera 1.17.3 to enhance the accuracy. Post-docking analyses and visualization of molecular interactions were performed using Discovery Studio 2024.[24,32,33]

3 Results and discussion

3.1. *In vitro* biological studies

3.1.1 *In vitro* thrombolytic test. The clot lysis assay revealed significant variations in fibrinolytic activity among *F. arabica* extracts and fractions. The butanol fraction demonstrated the

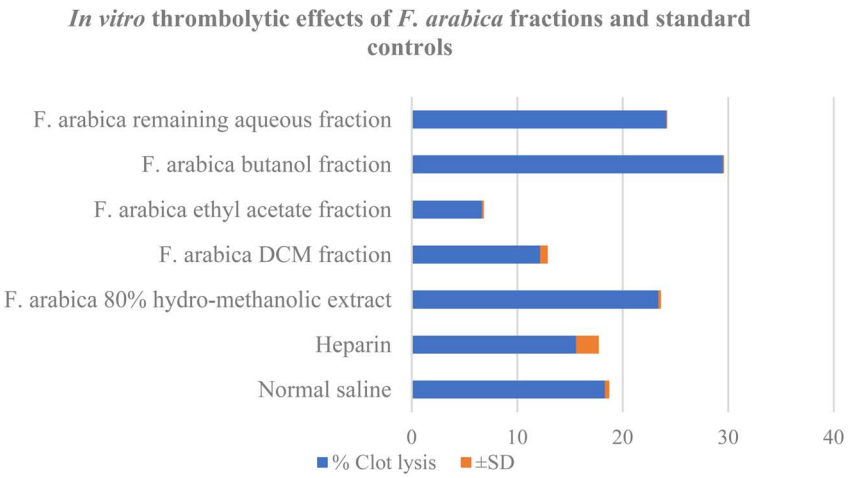

Fig. 2 *In vitro* thrombolytic effects of *F. arabica* fractions and standard controls.

highest activity (29.505 ± 0.095%), surpassing both the negative control (normal saline, 18.31%) and the reference anticoagulant heparin (15.575 ± 2.155%), suggesting the presence of potent thrombolytic compounds, likely polar secondary metabolites such as saponins. The 80% hydro-methanolic extract (23.385 ± 0.235%) and the remaining aqueous fraction (24.13 ± 0.09%) also exhibited notable activity, reinforcing the role of polar constituents in clot dissolution. In contrast, the ethyl acetate (6.655 ± 0.175%) and DCM (12.17 ± 0.73%) fractions showed markedly lower efficacy, indicating that nonpolar or mid-polar compounds may contribute minimally to fibrinolytic effects. The unexpected underperformance of heparin relative to plant extracts may reflect synergistic interactions among phytochemicals or assay-specific conditions (Table S1 and Fig. 2). These findings highlight the butanol fraction as a promising candidate for further isolation of bioactive anticoagulant agents, warranting detailed phytochemical and mechanistic investigations.[6]

3.1.2 *In vitro* anticoagulant test. The anticoagulant assay demonstrated concentration-dependent effects across *F. arabica* extracts, with the butanol fraction exhibiting the most potent activity, completely inhibiting clot formation at ≥40 mg mL^{-1}, comparable to the heparin control (no clot). The 80% hydro-methanolic extract and aqueous fraction showed moderate efficacy, respectively reducing clot weight by 0.0893 ± 0.02 g and 0.1289 ± 0.02 g at 100 mg mL^{-1}. The DCM and ethyl acetate fractions displayed weaker, inconsistent inhibition (*e.g.*, DCM: 0.2118 ± 0.095 g at 200 mg mL^{-1}). Notably, all fractions outperformed the negative control (saline, 0.3523 ± 0.13 g), confirming intrinsic anticoagulant properties (Table 1). The butanol fraction's superior activity suggests polar compounds (*e.g.*, saponins) as key bioactive agents,[6] while the diminished efficacy of non-polar fractions (DCM, ethyl acetate) implies limited solubility or inhibitory interactions. These findings align with prior clot lysis data, reinforcing the butanol fraction's therapeutic potential for further isolation of anticoagulant phytochemicals.

3.1.3 Effect of a saponin-rich fraction on plasma antithrombin-III activity using an *in vitro* quantitative immunoturbidimetric assay. The effect of the saponin-rich butanol fraction on plasma antithrombin-III (AT-III) activity was assessed *in vitro* using an immunoturbidimetric assay. The resulting AT-III concentrations and absorbance changes (ΔAbs) at different saponin concentrations are illustrated in Fig. 3.

The effect of varying concentrations of the saponin-rich fraction on Antithrombin-III concentration was evaluated. The standard sample, with no saponin, showed a ΔAbs of 0.012 and an Antithrombin-III concentration of 0.047 mg dL^{-1}. As the

Table 1 Concentration-response relationship of *F. arabica* hydro-methanolic extract and partitioned fractions in blood clot inhibition assays

Clot wt. Concentration	15 mg mL^{-1}	30 mg mL^{-1}	40 mg mL^{-1}	50 mg mL^{-1}	100 mg mL^{-1}	200 mg mL^{-1}
Total 80% hydro-methanolic extract	0.352 ± 0.04	0.3 ± 0.061	0.314 ± 0.03	0.2083 ± 0.01	0.0893 ± 0.02	No clot
DCM fraction	0.279 ± 0.012	0.274 ± 0.016	0.282 ± 0.02	0.1944 ± 0.03	0.2292 ± 0.01	0.2118 ± 0.095
Ethyl acetate fraction	0.266 ± 0.023	0.286 ± 0.011	0.25 ± 0.03	0.1742 ± 0.09	0.1642 ± 0.02	0.1896 ± 0.08
Butanol fraction	0.3587 ± 0.01	0.32 ± 0.034	No clot	No clot	No clot	No clot
Aqueous fraction	0.3 ± 0.05	0.32 ± 0.01	0.34 ± 0.04	0.1779 ± 0.01	0.2261 ± 0.09	0.1289 ± 0.02
Control (500 μL blood)	0.366 g ± 0.021					
−ve control (500 μL blood + 100 μL saline)	0.3523 g ± 0.13					
+ve control (25 μL heparin + 75 μL saline)	No clot formation					

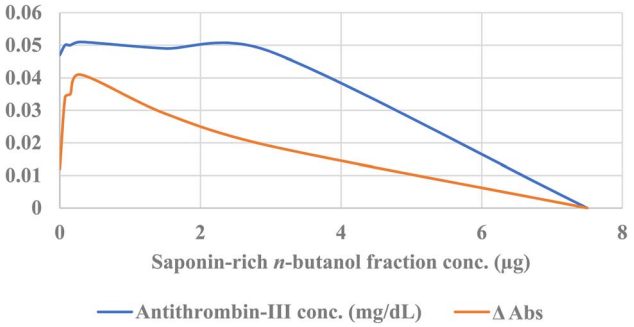

Fig. 3 Dose-dependent effects of saponin-rich *n*-butanol fraction on Δ absorbance and Antithrombin-III Levels.

saponin concentration increased to 0.075 µg and 0.15 µg, the ΔAbs values rose to 0.034 and 0.035, respectively, while the Antithrombin-III concentration remained relatively stable at 0.05 mg dL^{-1}. At 0.3 µg saponin, the ΔAbs increased further to 0.041, with a slight increase in Antithrombin-III concentration to 0.051 mg dL^{-1}. However, higher concentrations of saponin (1.5 µg and 3 µg) resulted in decreased ΔAbs values of 0.029 and 0.019, respectively, with Antithrombin-III concentrations of 0.049 mg dL^{-1} and 0.048 mg dL^{-1}. At the highest tested concentration of 7.5 µg, both ΔAbs and Antithrombin-III concentration dropped to zero, indicating a possible saturating effect at this level.

In the control sample (without plant extract), AT-III concentration was 0.047 mg dL^{-1} with a corresponding ΔAbs of 0.012. Upon addition of low saponin concentrations (0.075–0.30 µg), a slight but consistent increase in both AT-III concentration (0.050–0.051 mg dL^{-1}) and ΔAbs (0.034–0.041) was recorded. This initial rise represents the binding phase, during which saponin molecules interact with AT-III through hydrophobic and hydrogen bonding forces. Such interactions likely induce minor conformational rearrangements in the AT-III molecule, exposing its reactive center loop and enhancing its affinity for target proteases.

Due to the similarity in the anticoagulant effect of saponins and heparin, the standard anticoagulant agent, both compounds are capable of interacting with antithrombin-III (AT-III) and modulating its activity through specific binding mechanisms. The initial rise observed in the curve may be explained by the mechanism proposed by Rosenberg, who reported that heparin and AT-III interact in a stoichiometric ratio.[34] When heparin is present at suboptimal concentrations, two molecular species may form: the heparin-AT-III complex and free AT-III. Electrophoretic analysis revealed that the secondary AT-III peak exhibited greater electrophoretic mobility than native AT-III (in the absence of heparin), suggesting that these species correspond to AT-III molecules bound to varying amounts of heparin. Furthermore, both plasma samples and AT-III standards showed a gradual increase in relative mobility (Rf) with increasing heparin concentration up to 8 U mL^{-1}, consistent with progressive complex formation.[35]

As saponin concentration increases, the interaction transitions into an activation phase, reflected by a moderate enhancement of AT-III activity and a corresponding prolongation of activated partial thromboplastin time (aPTT) in parallel assays. This phase suggests that saponin binding may stabilize the active conformation of AT-III, thereby improving its anticoagulant efficiency.

At higher concentrations (≥1.5 µg), however, both AT-III concentration and ΔAbs begin to decline, reaching zero at 7.5 µg. This indicates a transition to the complete saturation phase, in which excessive saponin binding of all free AT-III occurs. The AT-III-saponin complex prevents antibody recognition in the immunoturbidimetric assay.

Our interpretation is supported by the findings of Chan *et al.* 1979, who reported that during radioimmunoassay (RIA), pre-incubation of heparin with AT-III standards led to a reduced ability of the heparin-AT-III complexes to bind AT-III antibodies. This observation suggests that heparin either masked the antibody recognition site or induced a conformational alteration in the AT-III molecule, thereby diminishing its immunoreactivity.[35]

Previous studies have proposed that heparin activates antithrombin-III (AT-III) by disrupting intramolecular salt bridges that stabilize its native conformation. Specifically, heparin binding releases interactions between helix D and β-sheet B, allowing structural rearrangements that generate an activated AT-III species capable of reactive loop insertion into β-sheet A and enzyme inhibition. This conformational transition explains the enhanced proteinase inhibitor activity observed upon heparin binding and the differential affinities among native, heparin-bound, and complexed AT-III forms.[36,37]

Previous studies have reported that saponins possess significant anticoagulant properties, including factor Xa (FXa) inhibitory activity and the presence of antithrombin-III (AT-III) – like active compounds. These bioactive constituents interfere with the formation of prothrombinase complexes, thereby slowing the conversion of prothrombin to thrombin. Consequently, saponins have been shown to prolong prothrombin time (PT), thrombin time (TT), and activated partial thromboplastin time (aPTT), while simultaneously reducing fibrinogen (Fib) levels.[38,39]

3.2. Encapsulation of *F. arabica* saponins from the butanol fraction in liposomal nanoparticles (the most biologically active fraction)

The nano formula of *F. arabica* saponins of the butanol fraction was found translucent, and it was clear after dilution with deionized water. The morphology of every liposome generated in this work was practically spherical in shape, well diffused, and less aggregated for enclosed vesicles, according to TEM images, as shown in Fig. 4.

3.2.1 Transmission electron microscope. The TEM results show that the mean size of the control liposomes was 214.786 ± 57.915 nm, while the mean size of the drug-loaded sample was 165.444 ± 47.352 nm. This indicates a noticeable reduction in liposome size following drug incorporation (Fig. 4).

The smaller average size of the drug-loaded liposomes compared to the control suggests that the encapsulated

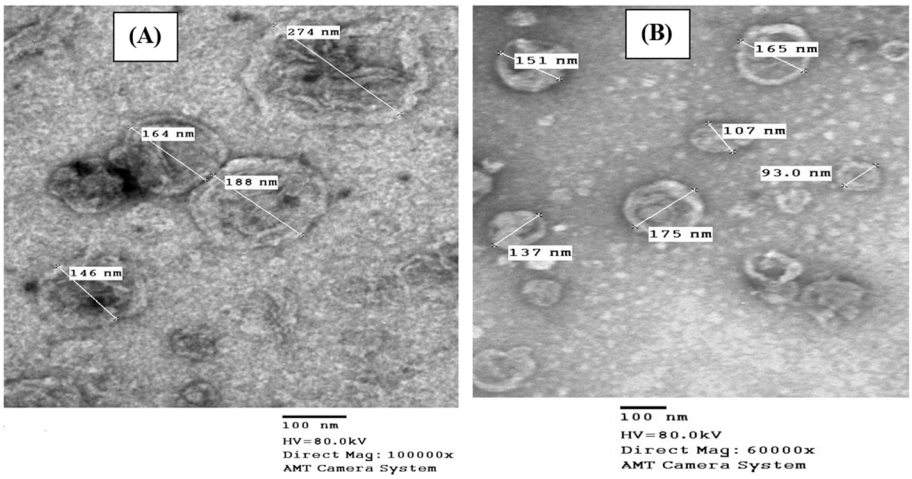

Fig. 4 TEM image for (A) empty Liposomes and (B) *F. arabica* saponins of butanol fraction-loaded liposomes.

compound (*F. arabica* saponins) may interact with the liposomal bilayer, promoting tighter lipid packing or compaction of the vesicles. This structural tightening can lead to reduced vesicle diameter, as observed. The decrease in size also supports the successful encapsulation of the active compound without disrupting the liposome morphology, aligning with a potentially more stable and efficient nano-delivery system.[40]

3.2.2 Particle size, polydispersity index (PDI) comparison and zeta potential of control and drug-loaded liposomes. Dynamic light scattering (DLS) measurements taken one week after preparation revealed that the *F. arabica* saponin-loaded liposomes maintained a smaller average particle size (218.2 ± 21.06 nm) compared to the control liposomes (243.4 ± 6.817 nm) Fig. 5. This sustained size difference suggests that the encapsulated saponins continue to interact with the liposomal bilayer over time, potentially promoting tighter lipid packing and maintaining vesicle compaction. The stability of the reduced size after one week indicates that the formulation resists significant aggregation or fusion.

The polydispersity index (PDI) also remained lower in the drug-loaded liposomes (0.388 ± 0.060) relative to the control (0.427 ± 0.019), indicating that the sample retained a more uniform size distribution over time. This points to long-term physical stability and consistency of the liposome population, an important characteristic for pharmaceutical and biomedical applications.

Moreover, the zeta potential of the drug-loaded liposomes remained slightly more negative (−19.6 ± 0.577 mV) than that of the control liposomes (−18.1 ± 0.100 mV). This increase in surface charge after one week suggests continued electrostatic repulsion between particles, which helps prevent aggregation and supports the colloidal stability of the formulation over time.

To sum up, the maintained particle size, reduced PDI, and more negative zeta potential of the *F. arabica* saponin-loaded

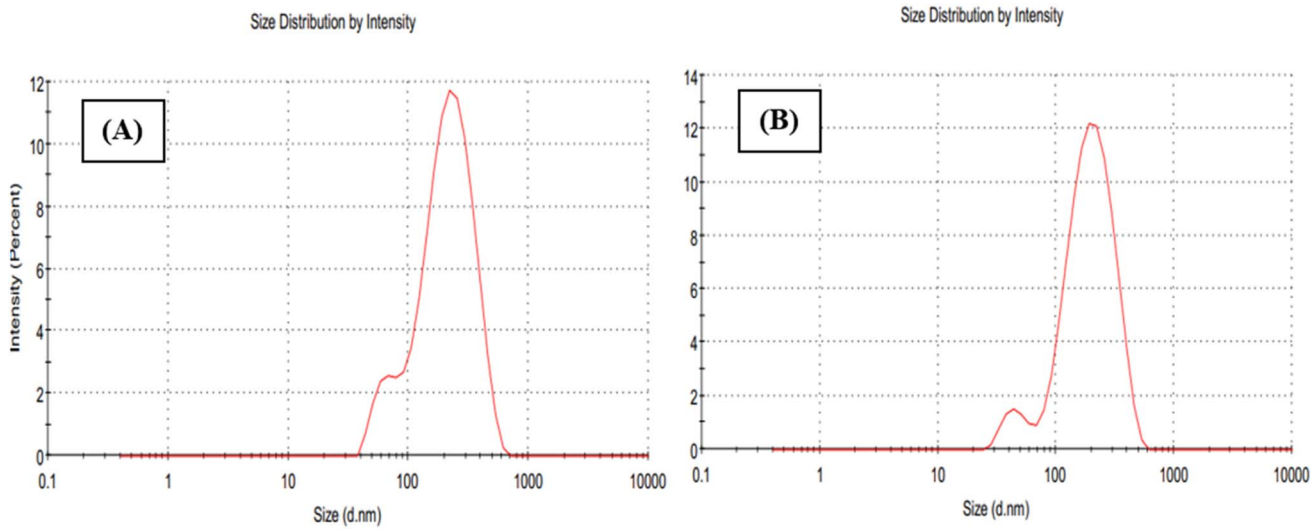

Fig. 5 Liposomes size distribution measured by dynamic light scattering (DLS) for (A) empty liposomes and (B) *F. arabica* saponins of butanol fraction-loaded liposomes.

Table 2 Particle size, Polydispersity Index (PDI) comparison and zeta potential of control and drug-loaded liposomes after one week of preparation

	Tested parameter	Test result
Control	Particle size	243.4 ± 6.817 nm
	PDI	0.427 ± 0.019
	Zeta potential	−18.1 ± 0.100 mV
Sample	Particle size	218.2 ± 21.06 nm
	PDI	0.388 ± 0.060
	Zeta potential	−19.6 ± 0.577 mV

liposomes one week after preparation confirm the stability and integrity of the formulation (Table 2). These results suggest that the nano-formulation remains physically stable, well-dispersed, and suitable for prolonged use in drug delivery systems.[41]

3.3. *Ex vivo* coagulation assay

The *ex vivo* coagulation assay revealed that the butanol fraction of *F. arabica* exerted significant dose-dependent anticoagulant effects (Table 3). The prothrombin time (PT) increased from 12 ± 2 s (baseline) to 30 ± 7 s (100 mg kg^{-1}) and 47 ± 3 s (200 mg kg^{-1}), demonstrating interference with the extrinsic coagulation pathway. More strikingly, the activated partial thromboplastin time (aPTT) exceeded 180 s at both doses (*versus* 37 ± 3 s in controls), indicating potent inhibition of the intrinsic pathway – an effect comparable to the liposome control (>180 s).

The results demonstrate that both the butanol fraction of *Fagonia arabica* and its liposomal nanoformulation significantly prolong coagulation parameters, as evidenced by increased PT and aPTT. Notably, the liposomal formulation at a low dose of 3 mg kg^{-1} achieved a PT of 35 ± 4 seconds and an aPTT exceeding 180 seconds, which is comparable to or exceeds the effects observed with higher doses (100 and 200 mg kg^{-1}) of the crude butanol extract. This indicates that liposomes offer superior anticoagulant efficacy at substantially lower doses. The enhanced performance is attributed to the ability of liposomes to improve the solubility, bioavailability, and targeted delivery of the active saponins, allowing for efficient interaction with coagulation pathways.[10] Additionally, the liposomal system may provide a sustained release effect, resulting in prolonged pharmacological action and more effective clot inhibition. The use of lower doses also suggests a reduced risk of systemic toxicity. Therefore, the liposomal formulation of *F. arabica* presents a more potent, efficient, and potentially safer alternative for anticoagulant and thrombolytic therapy compared to the crude extract.

The observed formation of only a "tiny clot" provides further evidence of robust anticoagulant activity. A smaller clot in non-citrated anticoagulated plasma compared to citrated plasma during PT/aPTT is expected and appropriate due to the stronger or irreversible inhibition of coagulation by non-citrate anticoagulants. This is why only citrated plasma is used for reliable coagulation testing. These findings corroborate previous *in vitro* results and suggest that the butanol fraction contains bioactive compounds (likely polar secondary metabolites) that either directly inhibit key coagulation factors (such as Xa or thrombin) or enhance endogenous anticoagulant pathways. The more pronounced effect on aPTT relative to PT implies a preferential action on the intrinsic and common pathways, possibly through interference with contact activation or thrombin generation. These results underscore the therapeutic potential of this fraction for conditions requiring anticoagulation, while highlighting the need for precise studies on its mechanism of action.

The observed anticoagulant effects of *F. arabica's* butanol fraction can be mechanistically attributed to its saponin content, which is characteristically enriched in polar fractions. The profound prolongation of aPTT (>180 s) suggests saponins interfere primarily with the intrinsic pathway, likely through: (1) direct inhibition of contact activation factors (FXII, FXI) *via* their amphipathic structures disrupting protein-membrane interactions, and/or (2) potentiation of antithrombin-III activity similar to heparinoids.[42] The dose-dependent PT prolongation (12 s → 47 s) implies additional inhibition of the common pathway, consistent with saponins' known ability to bind and inactivate thrombin (FIIa) and Factor Xa.[43] The complete clot inhibition aligns with reports that triterpenoid saponins form complexes with fibrinogen, preventing polymerization. These structure–activity relationships are characteristic of saponin-rich fractions, as evidenced by comparable effects of ginsenoside Ro, an oleanane-type saponin, which inhibited thrombin-induced platelet aggregation and reduced the binding of fibrinogen to αIIb/β3 *via* cAMP-dependent vasodilator-stimulated phosphoprotein phosphorylation.[7] The results strongly suggest that saponins are the principal bioactive constituents responsible for anticoagulant activity.

3.4. Chemistry

3.4.1 LC-MS peak characterization and tentative identification. The LC-MS analysis revealed several major peaks, each corresponding to potential triterpenoid saponins. The observed molecular ions, fragmentation patterns, and relative peak areas support tentative structural assignments as follows:

Table 3 Effect of *Fagonia arabica* butanol fraction and its liposomal formulation on coagulation parameters (PT and aPTT) in rats

Test	Before IP injection (self-control)	Liposomes (3 mg Kg^{-1})	Butanol fraction (100 mg kg^{-1})	Butanol fraction (200 mg kg^{-1})	Observation
PT	12 ± 2	35 ± 4 s	30 ± 7 s	47 ± 3	A tiny clot formed compared
aPTT	37 ± 3	>180	>180	>180	to the control

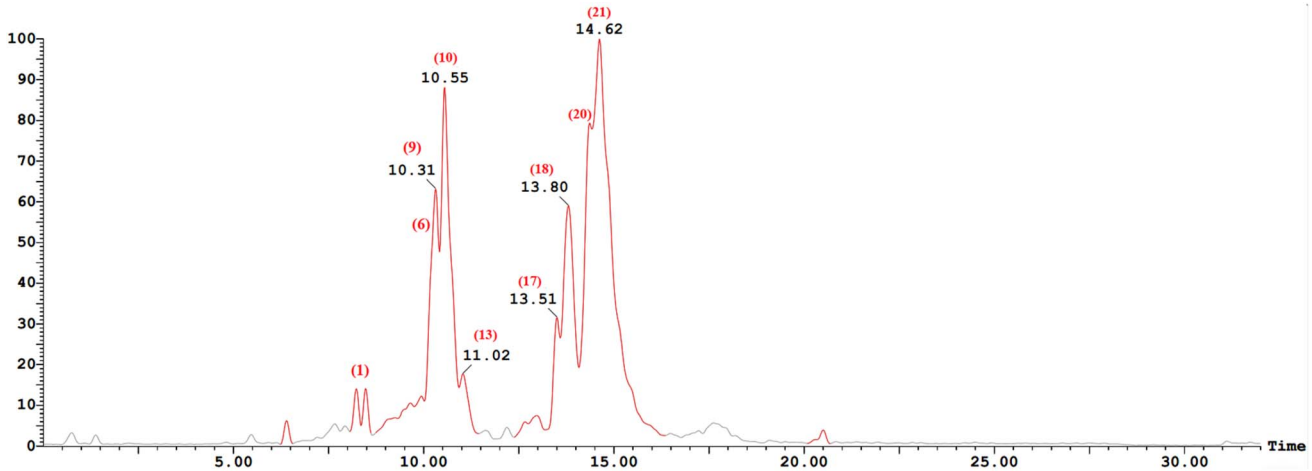

Fig. 6 Base Peak Intensity (BPI) chromatogram of saponin-enriched fraction of butanol fraction of *F. arabica* L. analyzed by LC-ESI-MS in negative ion mode.

Table 4 Tentatively identified saponins of saponin-enriched fraction of butanol fraction of *F. arabica* L. analyzed by LC-ESI-MS[a]

Peak no.	Rt (min)	Mode	*m/z*	Molecular formula	MS/MS	Tentatively identification	Reference
1	8.25	$[M]^-$	1106.4468	$C_{46}H_{76}Na_2O_{23}S_2$	553, 576, 979, 1060, 1083, 1106	OH-Ole or OH-Urs-pentose-pentose-hexose-2NaHSO$_3$	37
2	8.25	$[M]^+$	1044.1390	$C_{52}H_{84}O_{21}$	425, 438, 456, 457, 588, 720, 882, 1044	Ole or Urs-pentose-pentose-hexose-hexose	38 and 39
3	8.48	$[M + H]^+$	473.7996	$C_{30}H_{48}O_4$	275, 410, 425, 457, 473	OH-Ole or OH-Urs	38 and 39
4	9.56	$[M + 2H]^+$	1178.7228	$C_{57}H_{92}O_{25}$	457, 589, 752, 884, 1047, 1178	Ole or Urs-pentose-pentose-pentose-hexose-hexose	38 and 39
5	9.82	$[M + 2H]^+$	1046.0408	$C_{52}H_{84}O_{21}$	457, 914, 1046	Ole or Urs-pentose-pentose-hexose-hexose	38 and 39
6	9.95	$[M]^-$	1090.4667	$C_{46}H_{76}Na_2O_{22}S_2$	568, 1044, 1067, 1090	Ole or Urs-pentose-pentose-hexose-2NaHSO$_3$	37
7	10.04	$[M + 2H]^+$	914.2768	$C_{47}H_{76}O_{17}$	457, 590, 752, 914	Ole or Urs-pentose-hexose-hexose	38 and 39
8	10.20	$[M + 2H]^+$	1046.4785	$C_{52}H_{84}O_{21}$	457, 914, 1046	Ole or Urs-pentose-pentose-hexose-hexose	38 and 39
9	10.31	$[M]^-$	1124. 3516	$C_{52}H_{84}O_{24}S$	585, 958, 992, 1058, 1124	OH-Ole or OH-Urs-pentose-pentose-hexose-deoxyhexose-SO$_3$	37
10	10.55	$[M]^-$	992.2978	$C_{47}H_{76}O_{20}S$	519, 945, 992	OH-Ole or OH-Urs-pentose-hexose-deoxyhexose-SO$_3$	37
11	10.60	$[M]^+$	882.0330	$C_{46}H_{74}O_{16}$	438, 456, 588, 750, 882	Ole or Urs-pentose-pentose-hexose	38 and 39
12	10.93	$[M]^+$	750.0143	$C_{41}H_{66}O_{12}$	438, 456, 472, 604, 750	OH-Ole or OH-Urs-pentose-deoxyhexose	38 and 39
13	11.02	$[M]^-$	978.1902	$C_{46}H_{74}O_{20}S$	847, 930, 978	OH-Ole or OH-Urs-pentose-pentose-hexose-SO$_3$	37
14	11.48	$[M]^+$	456.3603	$C_{30}H_{48}O_3$	275, 319, 363, 456	Ole or Urs	38 and 39
15	12.73	$[M + H + Na]^+$	906.2057	$C_{46}H_{74}O_{16}$	457, 589, 721, 906	Ole or Urs-pentose-pentose-hexose	38 and 39
16	12.99	$[M + H + Na]^+$	905.9954	$C_{46}H_{74}O_{16}$	440, 559, 721 906	Ole or Urs-pentose-pentose-hexose	38 and 39
17	13.51	$[M]^-$	962.2296	$C_{46}H_{74}O_{19}S$	796, 962	Ole or Urs-pentose-pentose-hexose-SO$_3$	37
18	13.80	$[M]^-$	962.2624	$C_{46}H_{74}O_{19}S$	962	Ole or Urs-pentose-pentose-hexose-SO$_3$	37
19	14.35	$[M + H]^+$	914.1820	$C_{47}H_{76}O_{17}$	440, 458, 580, 750, 914	Ole or Urs-pentose-hexose-hexose	38 and 39
20	14.36	$[M]^-$	830.2686	$C_{41}H_{66}O_{15}S$	578, 830	Ole or Urs-pentose-hexose-SO$_3$	37
21	14.62	$[M]^-$	830.2686	$C_{41}H_{66}O_{15}S$	830	Ole or Urs-pentose-hexose-SO$_3$	37
22	14.66	$[M + H]^+$	914.1564	$C_{47}H_{76}O_{17}$	440, 458, 854, 914	Ole or Urs-pentose-hexose-hexose	38 and 39

[a] Abbreviations: Ole, Oleanolic acid; Rt, retention time; Urs, Ursolic acid.

(A) In negative electrospray ionization mode, the observed major peaks are sulfated triterpenoid saponins[44] (Fig. 6 and Table 4):

Peak 1 (Rt = 8.25 min), exhibits $[M]^-$ at *m/z* 1106.4468, which gives main fragments at *m/z* 553 $[472 + HSO_3]^-$, *m/z* 576 equivalent to sulfated hydroxylated sodium salt of oleanolic or ursolic acid $[472 + 81 + 23]^-$ with a trisaccharide chain comprising two pentoses and one hexose unit to give *m/z* 979 $[472 + 81 + 132 + 132 + 162]^-$, *m/z* 1060 $[472 + 81 + 132 + 132 + 162 + 81]^-$, *m/z* 1083 $[472 + 81 + 132 + 132 + 162 + NaHSO_3]^-$ and *m/z* 1106 $[472 + (2 \times 132) + 162 + 2NaHSO_3]^-$. Therefore, it's tentatively identified as the sodium salts of sulfated glycoside of hydroxylated oleanolic or ursolic acid, containing two pentose and one hexose unit (Fig. S1).

Peak 6 (Rt = 9.95 min) displays a molecular ion $[M]^-$ at *m/z* 1090.4667 corresponding to $[456 + (2 \times 132) + 162 + 2NaHSO_3]^-$. Therefore, it's tentatively identified as the sodium salts of sulfated glycoside of oleanolic or ursolic acid, containing two pentose and one hexose unit (Fig. S6).

Peak 9 (Rt = 10.31 min): Displays a molecular ion $[M]^-$ at *m/z* 1124. 3516, consistent with a sulfated, hydroxylated oleanolic or ursolic acid saponin (472 + 80 Da) with a tetrasaccharide chain comprising two pentoses (2 × 132 Da), hexose (162 Da), and deoxyhexose (146 Da) (Fig. S9).

Peak 10 (Rt = 10.55 min): exhibits $[M]^-$ at *m/z* 992.2978, consistent with a sulfated, hydroxylated oleanolic or ursolic acid saponin (472 + 80 Da) with a trisaccharide chain comprising pentose (132 Da), hexose (162 Da), and deoxyhexose (146 Da) (Fig. S10).

Peak 13 (Rt = 11.02 min), displays $[M]^-$ at *m/z* 978.1902, consistent with a sulfated, hydroxylated oleanolic or ursolic acid saponin (472 + 80 Da) with a trisaccharide chain comprising two pentoses (2 × 132 Da) and one hexose (162 Da) (Fig. S13).

Peak 17 (Rt = 13.51 min) (Fig. S17) and Peak 18 (Rt = 13.80 min) (Fig. S18) show $[M]^-$ at *m/z* 962, corresponding to a sulfated oleanolic or ursolic acid saponin with a trisaccharide composed of two pentoses and one hexose.

Peak 20 (Rt = 14.36 min) (Fig. S20) and Peak 21 (Rt = 14.62 min) (Fig. S21) share the same $[M]^-$ at *m/z* 830.2686, suggesting it is an isomer or closely related analog, differing possibly in sugar linkage or sulfation site. It is tentatively identified as a sulfated oleanolic or ursolic acid (456 + 80 Da) saponin bearing a disaccharide chain composed of pentose (132 Da) and hexose (162 Da).

(B) In positive electrospray ionization mode, depending on previous literature,[45,46] the observed peaks of triterpenoid saponins are (Fig. 7 and Table 4):

Peak 2 (Rt 8.25 min) displayed a molecular ion $[M]^+$ at *m/z* 1044.1390, corresponding to oleanolic or ursolic acid (456 Da) conjugated with two pentose (2 × 132 Da) and two hexose (2 × 162 Da) units. This mass suggests a pentose- and hexose-rich tetrasaccharide chain linked to the triterpenoid aglycone, consistent with a complex oleanane-type or ursolic saponin (Fig. S2).

Peak 3 (Rt 8.48 min) is proposed to correspond to hydroxylated oleanolic or ursolic acid $[M + H]^+$ at *m/z* 473, based on the observed mass increase consistent with a single hydroxyl modification of the aglycone (Fig. S3).

Peak 4 (Rt 9.56 min) showed a molecular ion $[M + 2H]^+$ at *m/z* 1178, which is consistent with a compound composed of oleanolic or ursolic acid (*m/z* 456) and a sugar moiety consisting of three pentoses (3 × 132 Da) and two hexoses (2 × 162 Da) (Fig. S4).

Peak 5 (Rt 9.82 min) (Fig. S5) presented a protonated ion $[M + 2H]^+$ at *m/z* 1046.0408, corresponding to oleanolic or ursolic acid (*m/z* 456) conjugated with two pentoses (2 × 132 Da) and two hexoses (2 × 162 Da), indicating a structurally related saponin with one fewer pentose than Peak 18.

Peak 7 (Rt 10.04 min) exhibited a molecular ion $[M + 2H]^+$ at *m/z* 914, indicative of a compound containing oleanolic or ursolic acid (*m/z* 456), one pentose (132 Da), and two hexoses (2 × 162 Da), forming a trimeric sugar chain (Fig. S7).

Peak 8 (Rt 10.20 min), as peak 20, showed a $[M + 2H]^+$ ion at *m/z* 1046, consistent with oleanolic or ursolic acid (*m/z* 456)

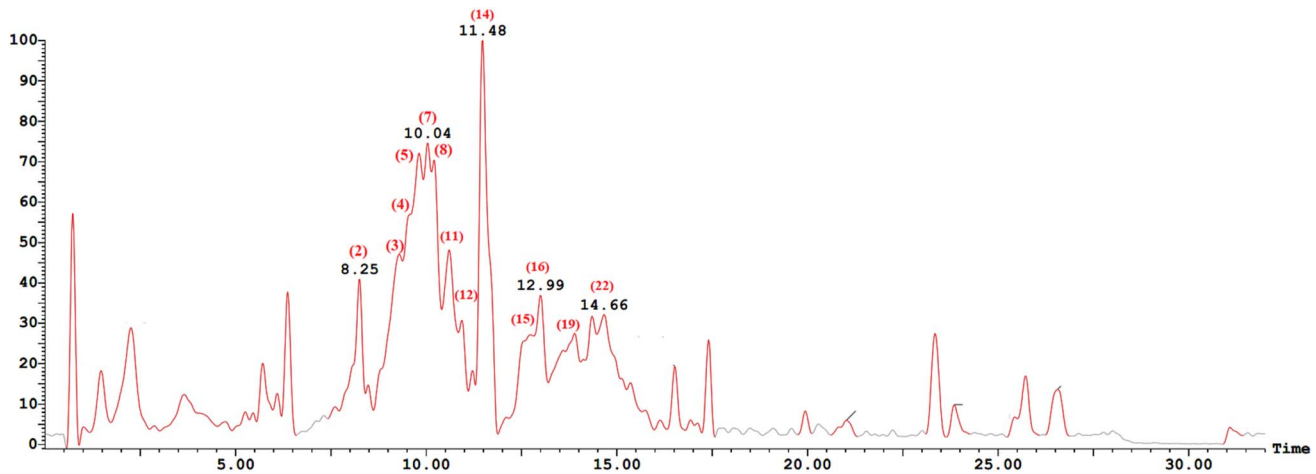

Fig. 7 Base Peak Intensity (BPI) chromatogram of saponin-enriched fraction of butanol fraction of *F. arabica* L. analyzed by LC-ESI-MS in positive ion mode.

attached to two pentoses (2 × 132 Da) and two hexoses (2 × 162 Da), suggesting a tetrasaccharide-conjugated triterpenoid saponin (Fig. S8).

Peak 11 (Rt 10.60 min) yielded a molecular ion $[M]^+$ at *m*/*z* 882, corresponding to oleanolic or ursolic acid (456 Da) conjugated with two pentoses (2 × 132 Da) and one hexose (162 Da), indicative of a trimeric sugar saponin (Fig. S11).

Peak 12 (Rt 10.93 min) exhibited an ion $[M]^+$ at *m*/*z* 750, corresponding to hydroxylated oleanolic or ursolic acid (472 Da) attached to a pentose (132 Da) and a deoxyhexose (146 Da). This suggests a saponin bearing a disaccharide composed of a pentose and deoxyhexose (Fig. S12).

Peak 14 (Rt 11.48 min) showed a precise mass of *m*/*z* 456 $[M]^+$, corresponding to oleanolic or ursolic acid, which suggests the presence of a free or non-conjugated triterpenoid aglycone (Fig. S14).

Peaks 15 (Rt 12.73 min) (Fig. S15) and 16 (Rt 12.99 min) (Fig. S16) displayed sodium adduct ions $[M + H + Na]^+$ at *m*/*z* 906, consistent with oleanolic or ursolic acid (*m*/*z* 456) conjugated with two pentoses (2 × 132 Da), one hexose (162 Da), and a sodium ion (23 Da). These peaks likely represent isomeric or closely eluting analogs.

Peaks 19 (Rt 14.35 min) (Fig. S19) and 22 (Rt 14.66 min) (Fig. S22) both exhibited $[M + 2H]^+$ ions at *m*/*z* 914, corresponding to oleanolic or ursolic acid (*m*/*z* 456) conjugated with one pentose (132 Da) and two hexoses (2 × 162 Da). These are likely isomeric saponins differing in sugar linkage or position.

Comprehensive profiling of the butanol fraction of *Fagonia arabica* using LC-qTOF-MS/MS enabled the tentative identification of 22 secondary metabolites, predominantly triterpenoid saponins (Table 4). The analysis was based on accurate mass measurements, retention times, molecular formulae, and diagnostic fragmentation patterns, and supported through comparison with published literature and spectral databases.[32]

The most frequently detected aglycones were oleanolic acid and ursolic acid, which are widely reported for their anti-inflammatory and antithrombotic properties. These triterpenoid cores were commonly glycosylated at positions C-3 and/or C-28, forming mono-, di-, tri- or tetra-saccharide chains or hydroxylated at C-23 or C-27 to give hydroxylated oleanolic acid or ursolic acid (Fig. 8).

3.4.2 Identification of isolated compounds of the butanol fraction. Given the significant pharmacological relevance of saponins, particular attention was directed toward *Fagonia arabica* L., which has been previously reported to possess saponins as major secondary metabolites. Accordingly, our study focused on the isolation and structural elucidation of these compounds. We confirmed one steroidal saponin and four terpenoidal saponins, which are the major saponins in the butanol fraction, by utilizing comprehensive spectroscopic analyses, including ^{1}H-NMR, APT, HSQC, and HMBC. We report for the first time the isolation and identification of β-sitosterol glucoside (**1**) from the butanol fraction of *F. arabica.*[47] In addition to these saponins, which were identified as 3-β-D-D-xylopyranosyl(**1** → **2**)–[β-D-glucopyranosyl (**1** → **3**)]-α-L-arabinopyranosyl 27-hydroxyoleanolic acid, 28-*O*-β-D-glucopyranoside (**2**), 3-*O*-β-D-xylopyranosyl (**1** → **2**)–[β-D-glucopyranosyl (**1** → **3**)-α-L-arabinopyranosyl 27-hydroxyursolicacid 28-*O*-β-D-glucopyranoside (**3**), 3-*O*-β-D-xylopyranosyl(**1** → **2**)–[β-D-glucopyranosyl(**1** → **3**)]-α-L-arabinopyranosyl oleanolic acid 28-*O*-β-D-glucopyranoside (**4**), and 3-β-D-xylopyranosyl(**1** → **2**)–[β-D-glucopyranosyl(**1** → **3**)]-α-L-arabinopyranosyl ursolic acid 28-*O*-β-D-glucopyranoside (**5**)[46] (Fig. S23). These saponins were concentrated within the butanol extract, which also exhibited the highest bioactivity among the tested fractions, thereby supporting a bioactivity-guided fractionation strategy.

The ^{1}H (400 MHz) (Fig. S24 and Table S2), ^{13}C NMR (101 MHz) (Fig. S25 and Table S2) and HSQC (Fig. S26) data of compound **1** in pyridine-d_5 revealed a steroidal glycoside structure, characterized by a Δ^5-unsaturated steroid core with a hydroxyl group at C-3 (δ_H 3.93, δ_C 78.28) and a *β*-D-glucopyranosyl moiety attached *via* an anomeric linkage (δ_H 5.05, d, J = 7.6 Hz; δ_C 102.37). Key HMBC correlations (Fig. S27) confirmed the steroidal framework, including methyl singlets at C-18 (δ_H 0.64, correlating with C-12, C-13, C-14, C-17) and C-19 (δ_H 0.92, correlating with C-1, C-5, C-9, C-10), as well as an olefinic proton at C-6 (δ_H 5.34, δ_C 121.71) adjacent to a quaternary carbon (C-5, δ_C 140.70). The side chain (C-20–C-29) exhibited a sitosterol-type structure with terminal ethyl (C-29, δ_H 0.87, t, J = 7.5 Hz) and methyl groups (C-26, C-27). The data collectively suggest a 3-*O*-β-D-glucopyranosyl sitosterol.

By comparing the NMR data of the four terpenoid saponins, compounds **2** to **5**, with those reported,[46] oleanolic acid and ursolic acid and their 27-OH were identified as the aglycones (Fig. S28–S33, Tables S3 and S5).

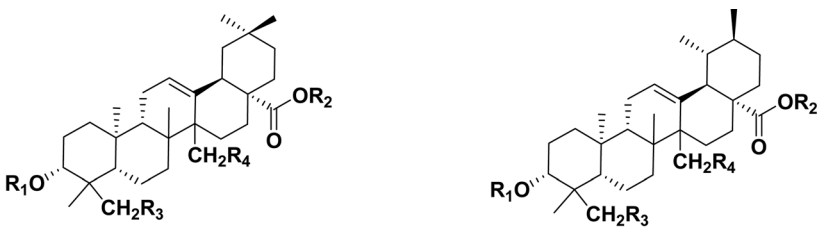

Oleanolic acid aglycone
R_1, R_2 glycosidic substitutions
R_3, R_4 = H or OH

Ursolic acid aglycone
R_1, R_2 glycosidic substitutions
R_3, R_4 = H or OH

Fig. 8 General triterpenoid aglycone structure of tentatively identified LC-ESI-MS/MS compounds.

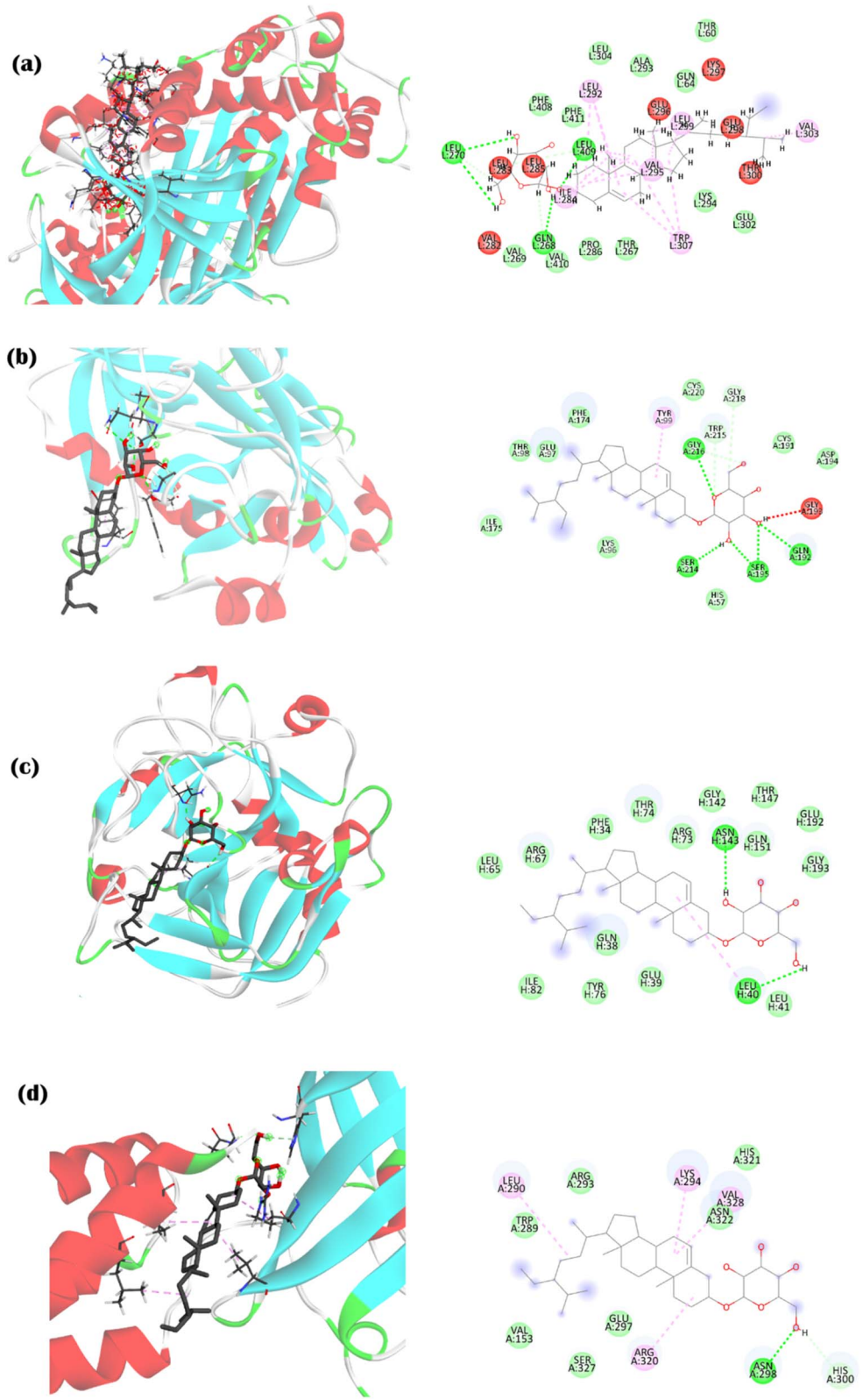

Fig. 9 3D and 2D docking representations of β-sitosterol glucoside with key anticoagulant enzymes: (a) Antithrombin III, (b) Factor Xa, (c) Thrombin (Factor IIa), and (d) VKORC1.

After being acid hydrolyzed, D-glucose, L-xylose and L-arabinose were isolated from the water layer by PTLC. From the coupling constants of the anomeric signals, the above four sugars were deduced to be β-configuration for xylose and glucose, and α for arabinose. By comparing with the aglycone in the ^{13}C NMR spectrum in C_5D_5N, δ 89.0 (C-3) and δ 176.2 (C-28)

were observed with distinct shift, indicating that sugar moieties were attached to these two positions. The carbon at δ 83.8 (C-3′) and δ 77.2 (C-2′) indicated that the glucose and the xylose were attached to positions 3 and 2 of the arabinose, respectively (Table S4).

The comparative analysis of the ^{13}C-NMR chemical shifts for oleanolic acid, ursolic acid, and their respective 27-hydroxy derivatives (27-OH oleanolic and 27-OH ursolic acids) (Table S5) reveals key structural distinctions, particularly in the aliphatic region of the triterpenoid skeleton. The most significant differences between oleanolic and ursolic acid lie in the chemical shifts of carbons C-18, C-19, C-20, C-21, C-22, C-29, and C-30. Notably, C-18 shows a pronounced downfield shift in ursolic acid (δ_C 53.1) compared to oleanolic acid (δ_C 41.5), reflecting stereochemical or conformational differences at ring D/E junctions. Similarly, C-19 shifts upfield in ursolic acid (δ_C 39.1) *versus* oleanolic acid (δ_C 46.8), likely due to the altered spatial orientation of the C-18 methyl group.

Upon hydroxylation at C-27, both derivatives (27-OH oleanolic and 27-OH ursolic acids) exhibit characteristic downfield shifts at C-27 (δ_C 64.2), confirming hydroxyl substitution. This modification also induces changes in neighboring carbons, such as shifts in C-14 (oleanolic: 46.0; ursolic: 48.1) and C-15 (δ_C 26.5) in the hydroxylated analogues, further supporting alterations in ring C conformation due to substitution. Finally, the downfield shifts at C-12 and C-13 in the 27-OH derivatives suggest minor perturbations in the olefinic region, likely from long-range electronic effects (Table S5). Collectively, these chemical shift variations provide clear NMR-based evidence to differentiate the four structurally related triterpenes.

3.5. Docking study

Anticoagulant drugs function by targeting critical components of the coagulation cascade, thereby preventing thrombus formation through inhibition of key enzymatic steps involved in thrombin and fibrin generation. Direct thrombin inhibitors, such as dabigatran, argatroban, and bivalirudin, specifically block thrombin (Factor IIa), while heparin exerts an indirect effect by potentiating antithrombin III, which inactivates thrombin. Similarly, Factor Xa, a pivotal enzyme in prothrombin activation, is inhibited directly by agents like rivaroxaban, apixaban, and edoxaban, or indirectly by unfractionated heparin and low-molecular-weight heparins (LMWHs) *via* antithrombin III. Additionally, warfarin impairs coagulation by inhibiting vitamin K epoxide reductase (VKOR), an enzyme required for recycling vitamin K, leading to reduced γ-carboxylation and subsequent synthesis of biologically active vitamin K-dependent clotting factors II, VII, IX, and X.[48]

Upon closer examination, Antithrombin, a plasma serpin, is mostly inactive as a coagulation protease inhibitor until it binds to heparan sulfate chains on the microvasculature. This binding occurs specifically to a core pentasaccharide, which is also present in therapeutic heparin. When antithrombin binds this pentasaccharide, it undergoes a structural change, as shown by a 2.9-Å structure of a dimer containing both latent and active antithrombin, each bound to the high-affinity pentasaccharide.

Table 5 Docking Scores of the five structurally elucidated compounds against anticoagulant, antiplatelet, and thrombolytic protein targets

	Anticoagulant targets				Antiplatelet targets			Thrombolytic targets	
Compounds/Targets	Thrombin (factor IIa)	Factor Xa	Antithrombin III	VKORC1	COX-1 (PTGS1)	$P2Y_{12}$	Phosphodiesterase III	Plasminogen	Tissue plasminogen activator (tPA)
3-*O*-β-D-glucopyranosyl sitosterol	−8.2	−8.0	−7.5	−8.9	−11.1	−8.5	−8.6	−7.6	−8.3
3-*O*-β-D-xylopyranosyl(**1** → **2**)-[β-D-glucopyranosyl(**1** → **3**)]-α-L-arabinopyranosyl oleanolic acid 28-*O*-β-D-glucopyranoside	−9.8	−9.9	−8.2	−10.2	−12.6	−9.5	−10.9	−10.4	−10.4
3-β-D-xylopyranosyl(**1** → **2**)-[β-D-glucopyranosyl(**1** → **3**)]-α-L-arabinopyranosyl ursolic acid 28-*O*-β-D-glucopyranoside	−9.8	−9.9	−8.2	−10.3	−13.0	−9.5	−10.9	−11.1	−10.2
3-β-D-xylopyranosyl(**1** → **2**)-[β-D-glucopyranosyl (**1** → **3**)]-α-L-arabinopyranosyl 27-hydroxyoleanolic acid, 28-*O*-β-D-glucopyranoside	−9.5	−9.7	−8.6	−9.6	−12.0	−9.2	−10.3	−10.6	−10.0
3-*O*-β-D-xylopyranosyl (**1** → **2**)-[β-D-glucopyranosyl (**1** → **3**)-α-L-arabinopyranosyl 27-hydroxyursolicacid 28-*O*-β-D-glucopyranoside	−9.5	−9.7	−8.6	−9.6	−12.5	−9.1	−10.7	−10.6	−9.8

This activation happens because the main β-sheet in antithrombin shifts from a partially six-stranded to a five-stranded form, causing the reactive center loop to move outward into a more exposed position. At the same time, helix D tilts and elongates, and a new two-turn helix P forms between helices C and D. These changes in shape at the heparin-binding site explain why antithrombin first binds tightly to heparan sulfates but later releases the antithrombin–protease complex into circulation. The pentasaccharide attaches through hydrogen bonds between its sulfate and carboxylate groups and specific amino acids: Arg-129 and Lys-125 on helix D, Arg-46 and Arg-47 on helix A, Lys-114 and Glu-113 on helix P, and Lys-11 and Arg-

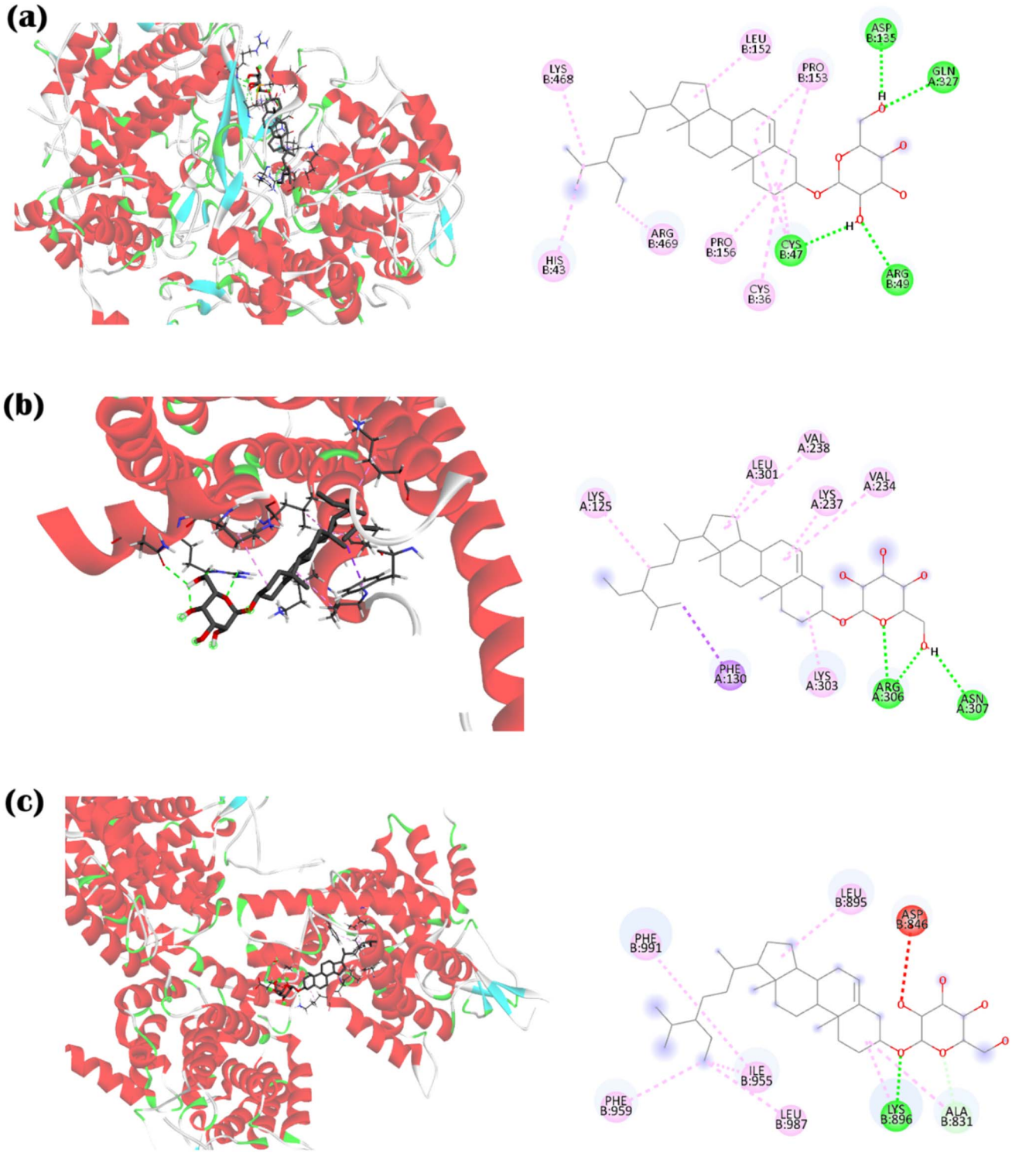

Fig. 10 3D and 2D docking representations of β-sitosterol glucoside with key Antiplatelet targets: (a) COX1, (b) $P2Y_{12}$, and (c) Phosphodiesterase III.

13 in a cleft near the amino terminus. Knowing this exact binding site helps in designing heparin analogues that more selectively target antithrombin, reducing side effects.[15] At the same binding site of the α-dimer of latent antithrombin III, our isolated compounds show even higher affinities, ranging from −7.5 to −8.6 (Fig. 9, 12(a) and Table 5).

Antiplatelet drugs act by inhibiting key pathways involved in platelet activation, aggregation, and cross-linking through the blockade of specific enzymes and receptors on the platelet surface. Cyclooxygenase-1 (COX-1) is irreversibly inhibited by aspirin, leading to reduced synthesis of thromboxane A_2, a potent platelet activator and aggregator. The $P2Y_{12}$ adenosine diphosphate (ADP) receptor, critical for sustained platelet activation, is selectively inhibited by agents such as clopidogrel, prasugrel, and ticagrelor, thereby attenuating ADP-mediated platelet aggregation. Additionally, phosphodiesterase (PDE) inhibitors like dipyridamole and cilostazol elevate intracellular cyclic adenosine monophosphate (cAMP) levels, which in turn suppress platelet activation and aggregation.[49]

As an illustrative example, P2Y receptors (P2YRs) are purinergic G-protein-coupled receptors (GPCRs) activated by extracellular nucleotides. Humans express eight functional P2YRs, grouped into $P2Y_1$-like and $P2Y_{12}$-like subfamilies. Their ligands are highly charged with low bioavailability and stability *in vivo*, limiting detailed characterization of this receptor family. $P2Y_{12}R$, activated by adenosine diphosphate (ADP), is crucial for platelet activation, granule secretion, and thrombus formation. Current antithrombotic drugs targeting $P2Y_{12}R$, such as clopidogrel, prasugrel, and ticagrelor, effectively prevent stroke and myocardial infarction but exhibit significant limitations, including prolonged effects and adverse side profiles.[19] Our isolated compounds display superior binding affinities for $P2Y_{12}R$, ranging from −8.5 to −9.5, highlighting their potential as improved therapeutic candidates (Fig. 10, 12(b) and Table 5).

Thrombolytic (fibrinolytic) agents facilitate the dissolution of intravascular thrombi by promoting the conversion of plasminogen into its active form, plasmin, a serine protease responsible for degrading fibrin, the structural framework of blood clots. This fibrinolytic activation is therapeutically enhanced by recombinant tissue plasminogen activators (tPAs) such as alteplase, reteplase, and tenecteplase, as well as by streptokinase, which indirectly forms an activator complex with plasminogen, thereby accelerating fibrin degradation and clot resolution.[50]

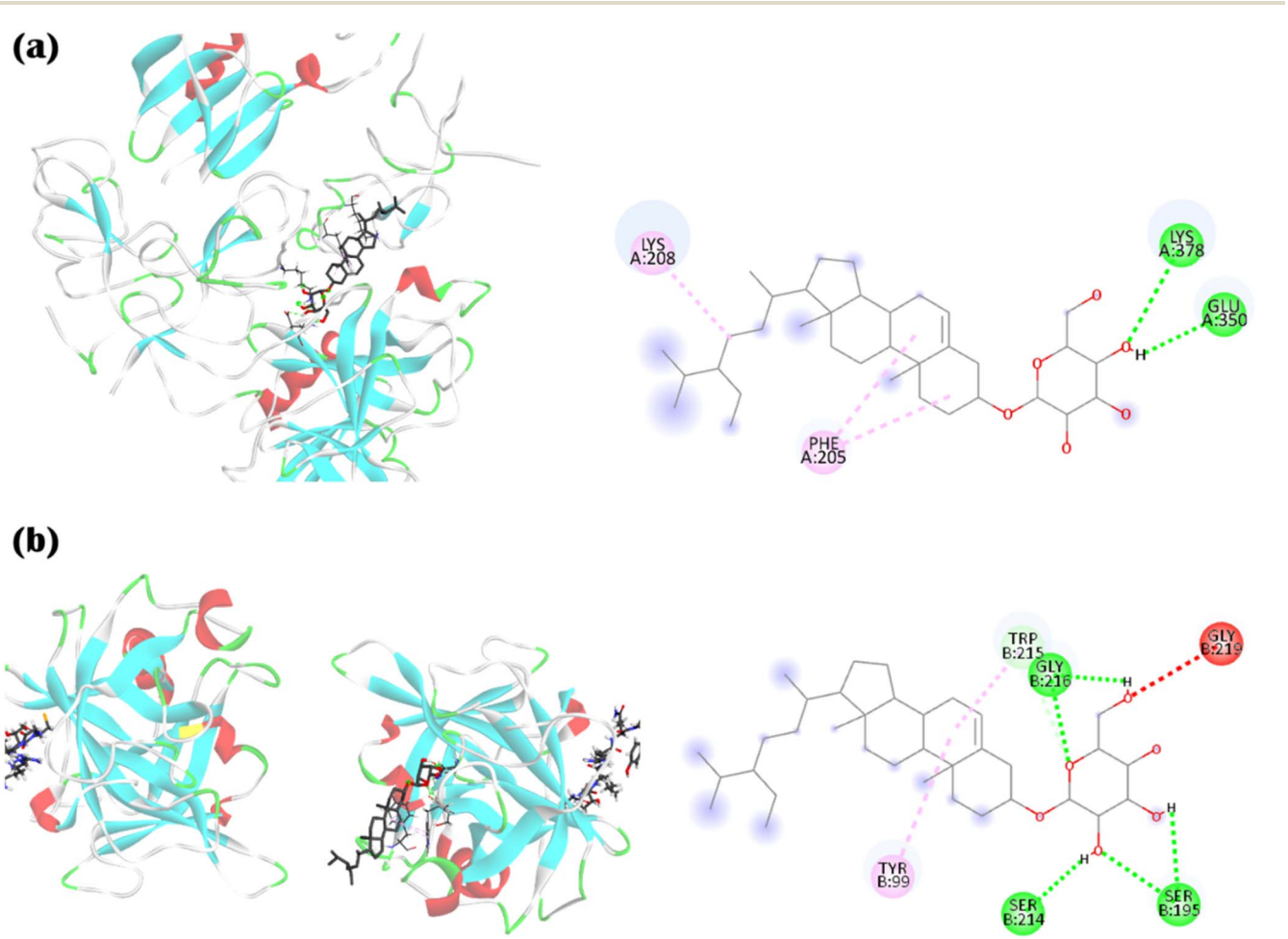

Fig. 11 3D and 2D docking representations of β-sitosterol glucoside with key thrombolytic targets: (a) plasminogen, (b) Tissue Plasminogen Activator (tPA).

Tissue-type plasminogen activator (tPA), a 60-kDa multidomain serine protease, catalyzes the conversion of plasminogen to plasmin, the rate-limiting step of the fibrinolytic cascade. Recombinant tPA is used clinically for acute myocardial infarction and pulmonary embolism due to its fibrin-dependent substrate specificity. Structurally, 187 residues of tPA correspond to α-chymotrypsin, with several key insertions forming the intermediate helix and surface loops around the active-site cleft that mediate substrate and inhibitor interactions. Remarkably, tPA cleaves only one physiological substrate bond in plasminogen (Arg560–Val561).[22] Our isolated compounds exhibit enhanced binding affinities for tPA, ranging from −8.3 to −10.5, highlighting their potential as improved therapeutic agents (Fig. 11, 12(c) and Table 5).

Our molecular docking analyses (Fig. 9–12 and Table 5) revealed that the primary determinant of binding affinity for the investigated glycosides is the sugar moiety rather than the aglycone scaffold. The glycosidic residues, particularly those linked to the 3-hydroxyl position, established extensive hydrogen bonding and polar interactions with key amino acid

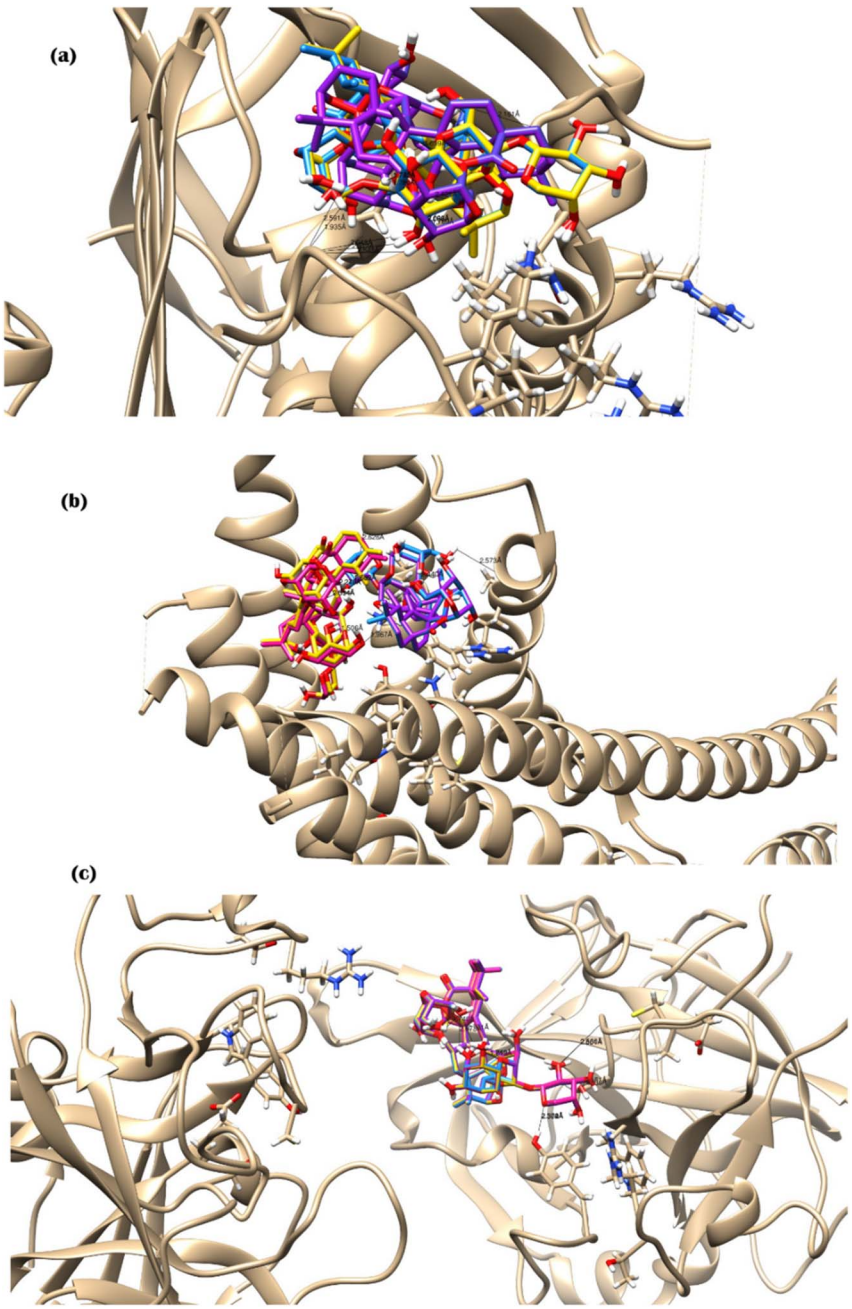

Fig. 12 Molecular docking of (a) Antithrombin III, (b) $P2Y_{12}$, (c) tissue-type plasminogen activator (tPA) with four identified terpenoid saponins. The docking results indicate multiple hydrogen bond interactions within the active-site cleft, supporting stable ligand conformations and strong binding affinities.

residues within the active or allosteric sites of the target proteins, thereby enhancing ligand stabilization. In contrast, β-sitosterol glucoside, containing a single sugar unit, exhibited comparatively lower binding affinity, underscoring the critical role of the glycosylation pattern in modulating protein-ligand interactions. Interestingly, the four terpenoid saponins demonstrated nearly equivalent binding affinities, suggesting that the carbohydrate portion dominates the interaction profile, while structural modifications of the aglycone, such as hydroxylation at the C-27 position or substitution between oleanolic and ursolic backbones, did not significantly alter binding strength. This observation highlights the importance of the hydrophilic sugar chains in mediating hydrogen bonding networks and optimizing steric complementarity with the protein binding pocket, whereas the hydrophobic aglycone primarily contributes to secondary interactions such as van der Waals contacts. Overall, these findings suggest that enhancing glycosylation complexity could be a key strategy to improve ligand affinity and selectivity for anticoagulant, antiplatelet, and thrombolytic targets.

Because thrombosis underlies several potentially fatal conditions, such as stroke, myocardial infarction, and pulmonary embolism, its prevention remains of critical importance.[10,11] To overcome the major limitations of conventional therapies, such as short plasma half-life, systemic toxicity, and an increased risk of bleeding, natural products and liposomal systems have emerged as promising strategies for the targeted delivery of antithrombotic and thrombolytic agents.[10] Previous studies have demonstrated that certain saponins influence prothrombin and other clotting factors, which play pivotal roles in the coagulation process.[8,9] Based on this, *Fagonia arabica*, known to be rich in triterpenoid saponins,[2] was selected for investigation. Liposomal formulations have also been reported to markedly enhance therapeutic efficacy[13] as they can preferentially accumulate at thrombus sites through receptor-mediated targeting or *via* the enhanced permeability and retention (EPR) effect. By reducing off-target effects and facilitating localized drug action, such targeted delivery minimizes systemic fibrinolysis and associated bleeding risks. Moreover, liposomal systems offer a versatile platform for improving the safety and efficacy of thrombolytic and anticoagulant therapies due to their adaptable formulation, enabling co-delivery of multiple agents and controlled release profiles.[14] Accordingly, we extended our work to identify the principal bioactive constituents responsible for the observed biological activity. The active compounds were characterized using LC-MS/MS and confirmed by NMR, and their interactions with coagulation-related proteins were further explored through molecular docking. To address the pathological challenge of thrombus formation and to promote the dissolution of pre-existing clots involved in life-threatening thromboembolic disorders, we focused on key molecular targets across the coagulation cascade, platelet activation pathways, and the fibrinolytic system in the docking study.

The novelty of the present study lies in integrating *in vitro*, *in vivo*, and *in silico* (molecular docking) approaches to identify and characterize the bioactive saponins of the *F. arabica*'s butanolic fraction and to elucidate their anticoagulant and thrombolytic mechanisms. Furthermore, the development of a liposomal nanoformulation of *F. arabica* butanol fraction represents a new strategy for enhancing the therapeutic potential, stability, and targeted delivery of its active compounds. Further in-depth *in vivo* investigations are recommended to validate and expand upon these findings.

4 Conclusion

In this study, we investigated the mechanism underlying the highly effective liposomal nano-encapsulation of *F. arabica* as a thrombolytic and anticoagulant herbal supplement. Its glycosylated terpenoids and steroids behave as amphiphilic molecules that preferentially integrate into the lipid bilayer. The hydrophobic aglycone aligns with phospholipid fatty acid chains, while the sugar moiety orients toward the polar headgroups, enhancing membrane compatibility without affecting surface charge. These compounds stabilize the bilayer by reducing fluidity, improving packing, and forming a hydration shell that minimizes vesicle fusion, resulting in smaller, uniform liposomes with enhanced stability and lower polydispersity. Embedded within the bilayer, their release is slow and diffusion-controlled, persisting until liposomal degradation occurs.

In addition, this study demonstrates the potent anticoagulant and thrombolytic properties of *Fagonia arabica* L., particularly its saponin-rich butanol fraction and its liposomal nanoformulation. Both *in vitro* and *in vivo* assays confirmed that the butanol extract and its liposomal formulation significantly prolonged coagulation times (PT and aPTT), indicating effective inhibition of the coagulation cascade, which was further approved by the docking study. Importantly, the liposomal formulation achieved the same biological activity, comparable or superior anticoagulant activity at a markedly lower dose (3 mg kg^{-1}) compared to the higher doses required for the crude butanol extract (100–200 mg kg^{-1}). LC-MS/MS profiling revealed a complex mixture of bioactive triterpenoid saponins, including oleanolic and ursolic derivatives with diverse sugar moieties and functional modifications, many of which are associated with the estimated biological activities. This underscores the enhanced efficacy and dose efficiency of the nanoformulated saponins, likely due to improved solubility, bioavailability, and sustained release properties of the liposomal system. Moreover, the absence of visible hemolysis during testing supports the safety and erythrocyte compatibility of the formulations. Collectively, these findings validate the traditional medicinal use of *F. arabica* and highlight the potential of liposomal nanoformulations as promising, low-dose, and safer antithrombotic agents for further pharmaceutical development.

Author contributions

A. R. H., M. S. A. and A. I. M.: methodology, investigation, review & editing, supervision, data curation and conceptualization, M. W. Sh.: methodology, investigation, and data curation of liposome nanoparticles study, A. M.:

methodology, investigation, and data curation of pharmacological studies, S. A. B: methodology, investigation, writing – review & editing, writing – original draft.

Conflicts of interest

The authors declare that they do not have any conflict of interest.

Data availability

Data is provided within the manuscript and the supplementary information (SI) file. Supplementary information is available. See DOI: https://doi.org/10.1039/d5ra06347g.

Abbreviations

aPTT	Activated partial thromboplastin time
DLS	Dynamic light scattering
HD_{50}	Hemolytic dose 50%
IP	intraperitoneal
PDI	Polydispersity index
PT	prothrombin time
PTLC	Preparative TLC
TEM	Transmission electron microscope
TLC	Thin-layer chromatography

References

1 R. N. Chopra and S. L. Nayar, Glossary of Indian Medicinal Plants. Council of Scientific and Industrial Research, *Q. Rev. Biol.*, 1956, **33**, 156, DOI: 10.1086/402350.
2 R. Satpute, R. Bhattacharya, R. S. Kashyap, H. J. Purohit, J. Y. Deopujari, G. M. Taori and H. F. Daginawala, Antioxidant Potential of *Fagonia arabica* against the Chemical Ischemia-Induced in PC12 Cells, *Iran. J. Pharm. Res.*, 2012, **11**(1), 303–313.
3 N. Iftikhar, S. Chatha, T. Ahmad, Q. Ali and A. Hussain, F. arabica L.: a review of its phytochemistry, pharmacology and traditional uses, *Comb. Chem. High Throughput Screen.*, 2022, **25**, 1187, DOI: 10.2174/1386207325666210923120957.
4 E. Baumann, G. Stoya, A. Völkner, W. Richter, C. Lemke and W. Linss, Hemolysis of Human Erythrocytes with Saponin Affects the Membrane Structure, *Acta Histochem.*, 2000, **102**, 21–35, DOI: 10.1078/0065-1281-00534.
5 K. Oda, H. Matsuda, T. Murakami, S. Katayama, T. Ohgitani and M. Yoshikawa, Adjuvant and Haemolytic Activities of 47 Saponins Derived from Medicinal and Food Plants, *Biol. Chem.*, 2000, **381**, 67–74, DOI: 10.1515/BC.2000.009.
6 S. G. Sparg, M. E. Light and J. van Staden, Biological Activities and Distribution of Plant Saponins, *J. Ethnopharmacol.*, 2004, **94**, 219–243, DOI: 10.1016/j.jep.2004.05.016.
7 B. Olas, K. Urbańska and M. Bryś, Saponins as Modulators of the Blood Coagulation System and Perspectives Regarding Their Use in the Prevention of Venous Thromboembolic Incidents, *Molecules*, 2020, **25**, 5171, DOI: 10.3390/molecules25215171.
8 L. Kang, J. Zhang, Y. Cong, B. Li, C. Xiong, Y. Zhao, D. Tan, H. Yu, Z. Yu, Y. Cong, C. Liu and B. Ma, Steroidal Glycosides from the Rhizomes of *Anemarrhena asphodeloides* and Their Antiplatelet Aggregation Activity, *Planta Med.*, 2012, **78**, 611–616, DOI: 10.1055/s-0031-1298223.
9 H.-C. Huang, W.-J. Tsai, C.-C. Liaw, S.-H. Wu, Y.-C. Wu and Y.-H. Kuo, Anti-Platelet Aggregation Triterpene Saponins from the Galls of *Sapindus mukorossi*, *Chem. Pharm. Bull.*, 2007, **55**, 1412–1415, DOI: 10.1248/cpb.55.1412.
10 T. A. Elbayoumi and V. P. Torchilin, Liposomes for Targeted Delivery of Antithrombotic Drugs, *Expert Opin. Drug Deliv.*, 2008, **5**, 1185–1198, DOI: 10.1517/17425240802497457.
11 A. M. Wendelboe and G. E. Raskob, Global Burden of Thrombosis: Epidemiologic Aspects, *Circ. Res.*, 2016, **118**, 1340, DOI: 10.1161/CIRCRESAHA.115.306841.
12 J. W. Weisel and J.-P. Collet, Packaging Is Important: Accelerated Thrombolysis with Encapsulated Plasminogen Activators, *J. Thromb. Haemost.*, 2004, **2**, 1545–1547, DOI: 10.1111/j.1538-7836.2004.00903.x.
13 J. L. Heeremans, R. Prevost, M. E. Bekkers, P. Los, J. J. Emeis, C. Kluft and D. J. Crommelin, Thrombolytic Treatment with Tissue-Type Plasminogen Activator (t-PA) Containing Liposomes in Rabbits: A Comparison with Free t-PA, *Thromb. Haemost.*, 1995, **73**, 488–494, DOI: 10.1055/s-0038-1653802.
14 V. K. Yadav, R. Gupta, A. A. Assiri, J. Uddin, A. A. Ishaqui, P. Kumar, K. M. Orayj, S. Tahira, A. Patel and N. Choudhary, Role of Nanotechnology in Ischemic Stroke: Advancements in Targeted Therapies and Diagnostics for Enhanced Clinical Outcomes, *J. Funct. Biomater.*, 2025, **16**, 8, DOI: 10.3390/jfb16010008.
15 X. Yu, Role and mechanism of heparin in cardiovascular system, *Discov. Appl. Sci.*, 2025, **7**, 341, DOI: 10.1007/s42452-024-05802-8.
16 D. J. P. Pinto, M. J. Orwat, S. Koch, K. A. Rossi, R. S. Alexander, A. Smallwood, P. C. Wong, A. R. Rendina, J. M. Luettgen, R. M. Knabb, K. He, B. Xin, R. R. Wexler and P. Y. S. Lam, Discovery of 1-(4-Methoxyphenyl)-7-Oxo-6-(4-(2-Oxopiperidin-1-Yl)Phenyl)-4,5,6,7-Tetrahydro-1H-Pyrazolo[3,4-c]Pyridine-3-Carboxamide (Apixaban, BMS-562247), a Highly Potent, Selective, Efficacious, and Orally Bioavailable Inhibitor of Blood Coagulation Factor Xa, *J. Med. Chem.*, 2007, **50**, 5339–5356, DOI: 10.1021/jm070245n.
17 S. Liu, S. Li, G. Shen, N. Sukumar, A. M. Krezel and W. Li, Structural Basis of Antagonizing the Vitamin K Catalytic Cycle for Anticoagulation, *Science*, 2021, **371**(6524), eabc5667, DOI: 10.1126/science.abc5667.
18 D. Picot and R. M. Garavito, The Structural Basis of Aspirin Activity Inferred From The Crystal Structure of Inactivated Prostaglandin H_2 Synthase, *Nat. Struct. Mol. Biol.*, 1995, **2**, 637, DOI: 10.1038/nsb0895-637.
19 K. Zhang, J. Zhang, Z.-G. Gao, D. Zhang, L. Zhu, G. W. Han, S. M. Moss, S. Paoletta, E. Kiselev, W. Lu, G. Fenalti, W. Zhang, C. E. Müller, H. Yang, H. Jiang, V. Cherezov,

V. Katritch, K. A. Jacobson, R. C. Stevens, B. Wu and Q. Zhao, Structure of the Human $P2Y_{12}$ Receptor in Complex with an Antithrombotic Drug, *Nature*, 2014, **509**, 115–118, DOI: 10.1038/nature13083.

20 G. Scapin, S. B. Patel, C. Chung, J. P. Varnerin, S. D. Edmondson, A. Mastracchio, E. R. Parmee, S. B. Singh, J. W. Becker, L. H. T. Van Der Ploeg and M. R. Tota, Crystal Structure of Human Phosphodiesterase 3B: Atomic Basis for Substrate and Inhibitor Specificity, *Biochemistry*, 2004, **43**, 6091–6100, DOI: 10.1021/bi049868i.

21 R. H. P. Law, T. Caradoc-Davies, N. Cowieson, A. J. Horvath, A. J. Quek, J. A. Encarnacao, D. Steer, A. Cowan, Q. Zhang, B. G. C. Lu, R. N. Pike, A. I. Smith, P. B. Coughlin and J. C. Whisstock, The X-Ray Crystal Structure of Full-Length Human Plasminogen, *Cell Rep.*, 2012, **1**, 185–190, DOI: 10.1016/j.celrep.2012.02.012.

22 M. Renatus, W. Bode, R. Huber, J. Stürzebecher, D. Prasa, S. Fischer, U. Kohnert and M. T. Stubbs, Structural Mapping of the Active Site Specificity Determinants of Human Tissue-Type Plasminogen Activator, *J. Biol. Chem.*, 1997, **272**, 21713–21719, DOI: 10.1074/jbc.272.35.21713.

23 F. Salama, M. A. El-Ghani and N. El-Tayeh, Vegetation and Soil Relationships in the Inland Wadi Ecosystem of Central Eastern Desert, Egypt, *Turk. J. Bot.*, 2013, 37, DOI: 10.3906/bot-1205-10.

24 S. A. Badawy, A. R. Hassan, R. H. Elkousy, S. A. Abu El wafa and A.-E. salam I. Mohammad, New Cyclic Glycolipids from *Silene succulenta* Promote in Vitro MCF-7 Breast Carcinoma Cell Apoptosis by Cell Cycle Arrest and in Silico Mitotic Mps1/TTK Inhibition, *RSC Adv.*, 2023, **13**, 18627–18638, DOI: 10.1039/D3RA01793A.

25 S. Prasad, R. S. Kashyap, J. Y. Deopujari, H. J. Purohit, G. M. Taori and H. F. Daginawala, Development of an *in Vitro* Model to Study Clot Lysis Activity of Thrombolytic Drugs, *Thromb. J.*, 2006, **4**, 14, DOI: 10.1186/1477-9560-4-14.

26 Química Clínica Aplicada S.A. (QCA Diagnostics), Antithrombin III (AT III) Quantitative Turbidimetry Kit-Spain: QCA Diagnostics, https://qca.es/en/antithrombin-iii/1564-antitrombina-iii-at-iii-25-ml-8430155003984.html, accessed November 2025.

27 M. H. Elsayed, M. W. Shafaa, M. S. Abdalla, M. F. El-Khadragy, A. E. A. Moneim and S. S. Ramadan, Antitumor Assessment of Liposomal Beta-Carotene with Tamoxifen Against Breast Carcinoma Cell Line: An *In Vitro* Study, *Biomolecules*, 2025, **15**, 486, DOI: 10.3390/biom15040486.

28 E. Amin, M. S. Abdel-Bakky, H. A. Mohammed, S. Chigrupati, K. A. Qureshi and M. H. A. Hassan, Phytochemical Analysis and Evaluation of the Antioxidant and Antimicrobial Activities of Five Halophytes from Qassim Flora, *Pol. J. Environ. Stud.*, 2022, **31**, 3005–3012, DOI: 10.15244/pjoes/145608.

29 D. N. Darlington, T. Craig, M. D. Gonzales, M. G. Schwacha, A. P. Cap and M. A. Dubick, Acute Coagulopathy of Trauma in the Rat, *Shock*, 2013, **39**, 440–446, DOI: 10.1097/SHK.0b013e31829040e3.

30 W. Wienen, J.-M. Stassen, H. Priepke, U. J. Ries and N. Hauel, *In-Vitro* Profile and *Ex-Vivo* Anticoagulant Activity of the Direct Thrombin Inhibitor Dabigatran and Its Orally Active Prodrug, Dabigatran Etexilate, *Thromb. Haemost.*, 2017, **98**, 155–162, DOI: 10.1160/TH07-03-0183.

31 H. El-Tantawy, *In Vitro, Ex Vivo*, Antiobesity Activity and Chemical Profiling of *Euclea racemosa* Subsp. Schimperi Aqueous Fraction, *Egypt. J. Bot.*, 2025, **65**, 332–349, DOI: 10.21608/ejbo.2024.309874.2954.

32 S. A. Badawy, A. R. Hassan, M. S. Abu Bakr and A. E.-S. I. Mohammed, UPLC-qTOF-MS/MS Profiling of Phenolic Compounds in *Fagonia arabica* L. and Evaluation of Their Cholinesterase Inhibition Potential through *in-Vitro* and *in-Silico* Approaches, *Sci. Rep.*, 2025, **15**, 5244, DOI: 10.1038/s41598-025-86227-0.

33 S. A. Badawy, A. R. Hassan, A. M. Korkor, M. S. Abu Bakr and A. E.-S. I. Mohammed, Metabolite Profiling of *Atriplex leucoclada* Boiss.: Exploring Its *In-Vitro* and *In-Silico* Cholinesterase Inhibition Potential by Molecular Modeling and ADMET Analysis, *Chem. Afr.*, 2025, **8**, 2773–2793, DOI: 10.1007/s42250-025-01304-1.

34 R. D. Rosenberg, Chemistry of the hemostatic mechanism and its relationship to the action of heparin, *Fed. Proc.*, 1977, **36**, 10–18.

35 V. Chan and T. K. Chan, Heparin-antithrombin III binding. *In vitro* and *in vivo* studies, *Haemostasis*, 1979, **8**(6), 373–389, DOI: 10.1159/000214328.

36 E. Ersdal-Badju, A. Lu, Y. Zuo, V. Picard and S. C. Bock, Identification of the antithrombin III heparin binding site, *J. Biol. Chem.*, 1997, **272**(31), 19393–19400, DOI: 10.1074/jbc.272.31.19393.

37 S. T. Olson, K. R. Srinivasan, I. Björk and J. D. Shore, Binding of high affinity heparin to antithrombin III: Stopped flow kinetic studies of the binding interaction, *J. Biol. Chem.*, 1981, **256**(21), 11073–11079.

38 Y. Ren, J. Ai, X. Liu, S. Liang, Y. Zheng, X. Deng and L. L. Chen, Anticoagulant active ingredients identification of total saponin extraction of different Panax medicinal plants based on grey relational analysis combined with UPLC-MS and molecular docking, *J. Ethnopharmacol.*, 2020, **260**, 112955, DOI: 10.1016/j.jep.2020.112955.

39 T. Dahmer, M. Berger, A. G. Barlette, J. Reck Jr, J. Segalin, S. Verza and G. Gosmann, G., Antithrombotic effect of chikusetsusaponin IVa isolated from *Ilex paraguariensis* (Maté), *J. Med. Food*, 2012, **15**(12), 1073–1080, DOI: 10.1089/jmf.2011.0320.

40 U. Baxa, Imaging of Liposomes by Transmission Electron Microscopy, in *Characterization of Nanoparticles Intended for Drug Delivery*, ed. S. E. McNeil, Springer, New York, NY, 2018, pp. 73–88, DOI: 10.1007/978-1-4939-7352-1_8.

41 M. Danaei, M. Dehghankhold, S. Ataei, F. Hasanzadeh Davarani, R. Javanmard, A. Dokhani, S. Khorasani and M. R. Mozafari, Impact of Particle Size and Polydispersity Index on the Clinical Applications of Lipidic Nanocarrier Systems, *Pharmaceutics*, 2018, **10**, 57, DOI: 10.3390/pharmaceutics10020057.

42 D. Gailani and T. Renné, The Intrinsic Pathway of Coagulation: A Target for Treating Thromboembolic

Disease?, *J. Thromb. Haemost.*, 2007, **5**, 1106–1112, DOI: **10.1111/j.1538-7836.2007.02446.x**.

43 A. Gómez-Outes, M. García-Fuentes and M. L. Suárez-Gea, Discovery Methods of Coagulation-Inhibiting Drugs, *Expert Opin. Drug Discov.*, 2017, **12**, 1195–1205, DOI: **10.1080/17460441.2017.1384811**.

44 A. Perrone, M. Masullo, C. Bassarello, A. I. Hamed, M. A. Belisario, C. Pizza and S. Piacente, Sulfated Triterpene Derivatives from *Fagonia arabica*, *J. Nat. Prod.*, 2007, **70**, 584–588, DOI: **10.1021/np060531m**.

45 E. A. El-Wakil, Phytochemical and Molluscicidal Investigations of Fagonia arabica, Z. Für Naturforschung C, 2007, **62**, 661–667, DOI: **10.1515/znc-2007-9-1006**.

46 T. Miyase, F. R. Melek, O. D. El-Gindi, S. M. Abdel-Khalik, M. R. El-Gindi, M. Y. Haggag and S. H. Hilal, Saponins from *Fagonia arabica*, *Phytochemistry*, 1996, **41**, 1175–1179, DOI: **10.1016/0031-9422(95)00725-3**.

47 T. Peshin and H. Kar, Isolation and Characterization of β-Sitosterol-3-*O*-β-D-Glucoside from the Extract of the Flowers of *Viola odorata*, *Br. J. Pharm. Res.*, 2017, **16**, 1–8, DOI: **10.9734/BJPR/2017/33160**.

48 P. Y. Kim, C. H. Yeh, B. J. Dale, B. A. Leslie, A. R. Stafford, J. C. Fredenburgh, J. Hirsh and J. I. Weitz, Mechanistic Basis for the Differential Effects of Rivaroxaban and Apixaban on Global Tests of Coagulation, *TH Open Companion J. Thromb. Haemost.*, 2018, **2**, e190–e201, DOI: **10.1055/s-0038-1649507**.

49 L. Stanger, A. Yamaguchi and M. Holinstat, Antiplatelet Strategies: Past, Present, and Future, *J. Thromb. Haemost.*, 2023, **21**, 3317–3328, DOI: **10.1016/j.jtha.2023.09.013**.

50 S. Hassanpour, H.-J. Kim, A. Saadati, P. Tebon, C. Xue, F. W. van denDolder, J. Thakor, B. Baradaran, J. Mosafer, A. Baghbanzadeh, N. R. deBarros, M. Hashemzaei, K. Lee, J. Lee, S. Zhang, W. Sun, H.-J. Cho, S. Ahadian, N. Ashammakhi, M. R. Dokmeci, A. Mokhtarzadeh and A. Khademhosseini, Thrombolytic Agents: Nanocarriers in Controlled Release, *Small*, 2020, **16**, 2001647, DOI: **10.1002/smll.202001647**.